INFLUENCE OF THE BIAXIALITY RATIO ON MULTIAXIAL FATIGUE OF METALLIC MATERIALS

A Thesis
Submitted to the Graduate Faculty
of the
North Dakota State University
of Agriculture and Applied Science

By

Charles Edward Adams

In Partial Fulfillment of the Requirements
for the Degree of
MASTER OF SCIENCE

Major Department:
Mechanical Engineering

April 2014

Fargo, North Dakota

North Dakota State University
Graduate School

Title

Influence of the Biaxiality Ratio on Multiaxial Fatigue of Metallic Materials

By

Charles Edward Adams

The Supervisory Committee certifies that this ***disquisition*** complies with North Dakota State University's regulations and meets the accepted standards for the degree of

MASTER OF SCIENCE

SUPERVISORY COMMITTEE:

Dr. Alan Kallmeyer
Chair

Dr. Ghodrat Karami

Dr. Fardad Azarmi

Dr. Siamak "Frank" Yazdani

Approved:

4/10/2014	Alan R. Kallmeyer
Date	Department Chair

ABSTRACT

The ability to model and predict multiaxial fatigue life without being too aggressive or conservative is of great interest to engineers. The purpose of this study was to examine the influence of the biaxiality ratio (σ_2/σ_1) on the multiaxial fatigue life of ductile metals. Fatigue models may exhibit significant variations in predicting the effect of the biaxiality ratio.

Two notch specimens with varying biaxiality ratios were machined and experimentally tested to check the validity of two different multiaxial fatigue models, an equivalent stress-based model (PSP) and a critical plane model (DP). The results indicated that a life benefit exists with an increasing biaxiality ratio, but that equivalent stress model can overpredict fatigue life with higher biaxiality ratios with no third principal stress present. A new critical plane model was proposed to account for secondary stresses in fatigue life prediction, and showed good experimental correlation with its theoretical fatigue life predictions.

ACKNOWLEDGEMENTS

This study was performed at the Materials Testing Laboratory at North Dakota State University in Fargo, North Dakota.

Special acknowledgement is given to Dr. Alan Kallmeyer for his wonderful patience, kindness, encouragement, and guidance throughout this study. His role as advisor provided many contributions to my development professionally, and personally throughout the last two years. Many thanks are extended to my committee members, Dr. Ghodrat Karami, Dr. Fardad Azarmi, and Dr. Frank Yazdani for their guidance and participation in this research. Acknowledgement is given to Shannon Viestenz and Gene Myrick for their technical support and help with the MTS load frame, and many thanks to the staff of the Department of Mechanical Engineering, with special regards for Tanya Erickson, Donna Alby, Chelsea Daley, and Tiffany Neuharth.

I would personally like to give many thanks to family and friends, with special consideration for my wife, Nyssa, who provided strong encouragement, support, and love throughout the last two years, while showing amazing patience throughout those long days and nights at the office. Also, my father and mother, Ed and Lonnie Adams, who pushed me hard to pursue my passion of engineering, work hard, and enjoy life's ride.

TABLE OF CONTENTS

LIST OF TABLES

LIST OF FIGURES

1. INTRODUCTION

Multiaxial fatigue is a phenomenon affecting components in many industries, including aerospace and automotive. Components subjected to multiaxial stress states present many challenges in developing proper parameters and methods for fatigue life estimation. In industries where design criteria, such as fail-safe or safe-life design, are critical for safety, predicting the fatigue life of components under multiaxial stress states is even more vital in insuring that parts are removed from service or don't fail before their designed fatigue life is reached. Conversely, conservative design methods to combat multiaxial fatigue can be costly by not utilizing the actual fatigue life effectively due to misunderstanding of multiaxial fatigue. As a result, understanding and accurately predicting fatigue life of components in multiaxial stress states is of vast importance to engineers, so that suitable designs are created to withstand the desired design life, without being too conservative.

Developing multiaxial fatigue parameters and methods presents many complications to overcome. Experimentally, subjecting test components to multiaxial stress states is difficult due to expensive costs and the complex nature of measuring stresses under multiaxial loading scenarios. Currently, only a small number of companies and universities have the facilities necessary to conduct true multiaxial fatigue testing. Due to this limitation, multiaxial fatigue studies on materials are generally uniaxial or torsional in nature, with extrapolation out to multiaxial fatigue loading conditions.

The last few decades have seen an increase in the number of studies performed on multiaxial fatigue, attempting to understand its mechanisms [1]. A variety of different methods have been developed, with three major classifications: equivalent stress/strain models, energy models, and critical plane models. The majority of the equivalent stress models use existing

static yield theories, such as the von Mises or Tresca criterion, with existing uniaxial stress life fatigue models such as the Goodman [2], or Gerber [3] models, with calculated equivalent stresses used to predict fatigue life. Equivalent strain models are used in a similar manner as the equivalent stress models, finding the strain amplitude and mean strain, but are instead used with strain-life models such as the Coffin-Manson model [4, 5]. Energy models typically use concepts such as distortion energy, or plastic work per cycle, to calculate fatigue damage, extrapolating out to predict fatigue life in multiaxial fatigue situations. Both of these methods use scalar parameters to predict fatigue life, allowing simple implementation. The major drawback of the equivalent stress/strain and energy models is their weak relationship with respect to actual, physical mechanisms of fatigue. Many of the equivalent stress/strain models cannot discern between the effects of out-of-phase loading versus in-phase loading, which can have significant influence on multiaxial fatigue life.

Experimental observations have shown that the nucleation of cracks in fatigue tends to occur on preferred planes, or orientations in the material, known as critical planes. Critical plane models have been developed the past few decades in order to capture this phenomenon and estimate fatigue lives of materials [6, 7, 8]. These models typically identify the critical plane as either the plane where a predetermined value is largest, such as maximum shear strain range, or where the greatest amount of damage occurs during the loading cycle. The major advantage of critical plane models is their ability to characterize in-phase and out-of-phase loading cycles, and better represent physical mechanisms of multiaxial fatigue than equivalent stress or energy models. In previous studies, critical plane models have been shown to provide a better correlation of multiaxial fatigue to uniaxial & torsion data than other methods [6, 9, 10].

Naturally, many of the multiaxial fatigue studies in the past have been completed using specimens that were smooth, and did not have major geometric notches or boundaries. Multiaxial fatigue in notched components introduces complexities including changes in the principal stress directions, and the stress gradient through the specimen. Most multiaxial fatigue notch adjustments are made as a notch factor and are either done through a critical point method, or a critical volume method [11, 12, 13]. Greater examination of the biaxiality ratio, σ_2/σ_1, must be considered, as equivalent stress models and critical plane models predict different fatigue lives as the biaxiality ratio departs from zero. Notches in uniaxial fatigue specimens naturally induce multiaxial stress states, which will influence the fatigue life estimation of different theories.

A review of multiaxial fatigue literature and detailed analysis of notch specimens is presented in this study. The main objective of this research is to examine a proposed critical plane model and an equivalent stress model, while comparing the correlation to experimental data of Direct Age 718 (DA 718) notch specimens with biaxiality ratios greater than zero. Special attention is given to the biaxiality ratio under low cycle fatigue to transition conditions, and the stress gradient in the specimens.

2. LITERATURE REVIEW

Presented in this chapter is a review of available literature with respect to multiaxial fatigue. The main focus is multiaxial fatigue models, with attention to notches.

2.1. Multiaxial Fatigue

Multiaxial fatigue occurs when components experience stress in multiple directions repeatedly, unlike uniaxial stress which occurs only in one principal direction. Over the last century, much research and development has been devoted to better understanding fatigue, and how it relates to uniaxial stress situations. It was recognized early, however, that extending uniaxial fatigue parameters to calculate multiaxial fatigue life proved inadequate for accurate prediction. Therefore, multiaxial models were developed to more accurately predict fatigue life. This is especially important for many industries that encounter multiaxial fatigue in their components, such as gas turbine disks, blades, axles, and shafts, as examples. Multiaxial fatigue modeling can generally be divided into three difference categories: equivalent stress/strain models, energy models, and critical plane models [8]. Each model family has advantages, and disadvantages with respect to actual physical representation, scalar values, and the ability to handle non-proportional loading.

2.1.1. Proportional versus Non-Proportional Loading

Multiaxial fatigue loading scenarios are sorted into two different categories. Proportional loading occurs when the principal stress directions during the loading cycle remain in a fixed orientation with the ratios between the principal stresses remaining constant. Therefore, the principal stresses reach their maximum and minimum at the same time. Non-proportional loading occurs if the principal stress directions change orientation throughout the loading cycle with changing ratios of the principal stresses as well.

The ability to test multiaxial fatigue specimens can be expensive and time consuming, especially when comparing proportional and non-proportional loading of materials. For example, Morrow [14] investigated Inconel 718 and its behavior under proportional and non-proportional loading using a tension-torsion machine to simulate these loading conditions. Only a small number of laboratories have the ability to simulate multiaxial fatigue testing without introducing notches or other stress raisers into the specimens.

Predicting fatigue life for components that undergo multiaxial, non-proportional loading provides additional challenges for theoretical modeling. Equivalent stress/strain models are generally only accurate for proportional loading scenarios, and have difficulty dealing with non-proportional loading. Energy models can provide for non-proportional loading, but are typically scalar in nature, not having much physical meaning. Critical plane models can account for non-proportional loading, and are modeled based upon physical mechanisms of fatigue crack nucleation. Currently, critical plane models have been seen as very promising due to their unique ability to handle various multiaxial loading scenarios.

2.2. Multiaxial Fatigue Modeling

From the mid-20th century onward, numerous multiaxial fatigue models have been developed to predict fatigue life of components. The first two methods, equivalent stress/strain and energy, will be discussed briefly, while critical plane models will receive more focus. These three methods discussed are based mainly upon crack nucleation, and fracture mechanics approaches, though important, will not be discussed in this review.

2.2.1. Equivalent Stress Models

Equivalent stress models are generally formed as extensions to classic static yield theories, with parameters found to be used with uniaxial fatigue models such as Goodman's [2]

model or Gerber's model [3]. Under high cycle fatigue (HCF) scenarios, equivalent stress models are typically used since crack nucleation consumes the majority of the fatigue life, and plasticity is not largely present. Two criteria often used are the maximum shear stress (Tresca) theory, and the octahedral shear stress (von Mises) theory. Their main objective is to reduce the multiaxial stress states into parameters that can be used with uniaxial fatigue models.

The first parameter that is typically calculated for equivalent stress models is the equivalent stress amplitude. The two equations shown below are the maximum shear stress theory, and the octahedral shear stress theory, respectively.

$$S_{qa} = S_{a1} - S_{a3} \tag{2.1}$$

$$S_{qa} = \frac{1}{\sqrt{2}}\sqrt{(S_{a1} - S_{a2})^2 + (S_{a2} - S_{a3})^2 + (S_{a1} - S_{a3})^2} \tag{2.2}$$

S_{qa} is the equivalent stress amplitude, and S_{a1}, S_{a2}, S_{a3} are the principal stress amplitudes. The maximum principal stress approach has shown better data correlation with brittle materials, while the octahedral shear stress approach, equation 2.2, has shown better data correlation with ductile materials [8].

If the loads are not completely reversed in all principal stress directions, then an equivalent mean stress term is commonly used to compensate for the mean stress effects. The most common method used is the sum of the principal mean nominal stresses, or first invariant of the mean stress tensor, shown below in equation 2.3.

$$S_{qm} = S_{m1} + S_{m2} + S_{m3} \tag{2.3}$$

S_{qm} is the equivalent mean nominal stress, and S_{m1}, S_{m2}, S_{m3} are the principal mean nominal stresses. Octahedral mean stress terms can be used, replacing equation 2.1 with principal mean nominal stresses instead of the principal stress amplitudes. However, the mean stress term is strongly reliant upon sign, and the octahedral stress is a scalar, equivalent term that is always

positive. If the mean stresses are truly negative in nature, then the octahedral stresses would permit underestimation of fatigue life, since compressive stresses on ductile metals generally provide a fatigue life benefit. Therefore, the sum of the principal mean stresses is used, as in equation 2.3.

Another commonly used method was proposed by Sines [15]. This method uses the principal mean nominal stresses and principal stress amplitudes to develop a fatigue strength value, shown below.

$$S_{N_f} = \frac{1}{\sqrt{2}}\left[\sqrt{(S_{a1} - S_{a2})^2 + (S_{a2} - S_{a3})^2 + (S_{a1} - S_{a3})^2} + m(S_{m1} + S_{m2} + S_{m3})\right] \quad (2.4)$$

S_{N_f} is the fully reversed uniaxial fatigue strength, and m is the coefficient of mean stress influence.

The equivalent stress models outlined should only be used for proportional loading scenarios, since equations 2.1 thru 2.4 are based upon the principal stress directions remaining unchanged throughout the loading cycle. Researchers have proposed modifications to account for different effects such as temperature, and material changes such as plasticity, and residual stress effects. Over the last few decades, these models have remained relatively unchanged.

2.2.2. Equivalent Strain Models

Equivalent strain models have been developed primarily for low cycle fatigue (LCF) situations. This is primarily due to stresses reaching beyond the yield strength of the material, making strain-based parameters more reliable for fatigue life estimation. The approach in equivalent strain models is very similar to equivalent stress models, but instead the parameters are used in common strain-life equations.

The equivalent strain amplitude parameter is typically found by using the maximum shear strain theory, or the octahedral shear strain theory. The equations for the maximum shear strain

theory, and the octahedral shear strain theory, respectively, are below. Similar to the equivalent stress amplitude terms, the maximum principal strain theory is typically used for brittle materials, while the octahedral shear strain theory is typically used for ductile materials.

$$\varepsilon_{qa} = \frac{\varepsilon_{a1} - \varepsilon_{a3}}{1+\upsilon} \tag{2.5}$$

$$\varepsilon_{qa} = \frac{\sqrt{(\varepsilon_{a1} - \varepsilon_{a2})^2 + (\varepsilon_{a2} - \varepsilon_{a3})^2 (\varepsilon_{a1} - \varepsilon_{a3})^2}}{\sqrt{2}(1+\upsilon)} \tag{2.6}$$

ε_{qa} is the equivalent strain amplitude, $\varepsilon_{a1}, \varepsilon_{a2}, \varepsilon_{a3}$ are the principal strain amplitudes, and υ is Poisson's ratio of the material. After the equivalent strain amplitude is calculated, it is substituted for the strain amplitude term, such as in the strain-life equation, shown below.

$$\varepsilon_{qa} = \frac{\sigma_f'}{E}\left(2N_f\right)^b + \varepsilon_f'\left(2N_f\right)^c \tag{2.7}$$

σ_f' is the fatigue strength coefficient, E is the modulus of elasticity, $2N_f$ is the number of reversals, b is the fatigue strength exponent, ε_f' is the fatigue ductility coefficient, and c is the fatigue ductility exponent. The equivalent strain amplitude parameter can be used in conjunction with other parameters such as the Smith Watson Topper (SWT) parameter [16]; however, if a considerable amount of plasticity occurs, stress relaxation can be introduced, which can add a fatigue life benefit to the component.

Related to the equivalent stress models, the equivalent strain models are best for proportional loading scenarios, and not adept to handling non-proportional loading. In order to handle non-proportional loading scenarios, different models must be considered.

2.2.3. Energy Models

Energy models are similar to equivalent stress and strain models, as the stress and strain histories are used to find a scalar parameter per loading cycle to compute fatigue life [17].

Fatigue life is computed by summing the fatigue damage per cycle, and relating this damage to other parameters.

In one of the more commonly accepted models, Garud [18] sought to apply hysteresis loop effects to multiaxial fatigue. The plastic work per cycle is examined by splitting the work into intervals. The plastic work is then summed per cycle, and used to calculate the fatigue life. Equation 2.8 below shows the plastic work per cycle.

$$\Delta W_c = \int_{cycle} \sigma_{ij} d\varepsilon_{ij}^p = \sum_{cycle} \Delta W_p = f(N) \tag{2.8}$$

ΔW_c is the total plastic work per cycle, σ_{ij} is the stress tensor, ε_{ij}^p is the plastic strain tensor, and ΔW_p is the total plastic work per increment. The total plastic work per cycle is related to a parameter to calculate fatigue life. This approach to multiaxial fatigue life estimation has shown promise in correlating material data [19]. However, the plastic work per cycle is a scalar quantity, which doesn't necessarily give physical meaning to crack initiation. This approach can be appropriate for proportional and non-proportional loading scenarios, but in HCF situations plastic work per cycle is extremely low or nonexistent, rendering this approach very difficult to use for fatigue life estimation.

Looking to account for HCF and mean stress effects, Ellyin and Kujawski [20] developed a model based upon the total strain energy density per cycle. By using the energy input, accounting for elastic and plastic strain energy, the total fatigue life could be estimated by including mean stress effects. Equations 2.9 and 2.10 below show the approach if traditional strain life fatigue properties are used.

$$\Delta W_t = \int_{cycle} \sigma_{ij} d\varepsilon_{ij}^p + \int_{cycle} H(\sigma_i) H\left(d\varepsilon_{ij}^e\right) \sigma_i d\varepsilon_i^e \tag{2.9}$$

$$\Delta W_t = 4\sigma_f' \varepsilon_f' \left(\frac{c-b}{c+b}\right) \left(2N_f\right)^{b+c} + \frac{{\sigma_f'}^2 \left(2N_f\right)^{2b}}{2E} \tag{2.10}$$

H(x) is the Heaviside function, σ_i is the first order principal stress tensor, ε_{ij}^e is the elastic strain tensor, and ε_i^e is the positive portion of the first order principal elastic strain tensor throughout the cycle. This method can be used for HCF fatigue situations since it accounts for elastic strain energy during the loading cycle. The scalar quantity doesn't convey any particular physical meaning, as is common with other energy methods.

Energy methods generally have not been widely accepted due to the scalar nature of the models, and the lack of physical resemblance. These methods can be used to account for non-proportional loading, however computationally it can be difficult, especially if the loading cycle is very complex.

2.2.4. Critical Plane Models

Critical plane models are the major third type of multiaxial fatigue criteria developed during the last century for predicting crack nucleation. Experimental data has shown that fatigue cracks generally nucleate on orientations called critical planes. These planes are typically where shear stress/strain or normal stress/strain amplitudes are at a maximum, depending on the material and nature of the loading cycle. The definition of where the critical plane is located and what its critical value is can vary between models. Some models are based mainly on stress related terms while others are based on strain related terms. Many of the newer critical plane models are hybrids of both stress and strain terms.

Brittle materials generally initiate cracks on critical planes where tensile stress and strain amplitude are both maximum. Many brittle materials, such as cast iron, have been observed to have this behavior. Once the tensile stress and/or strain amplitude are calculated, the parameters are related to uniaxial fatigue data to calculate fatigue life.

Ductile materials develop and initiate cracks more often on critical planes where maximum shear stress and strain amplitudes are present. The normal stress and strain on the critical plane can encourage crack nucleation in combination with the shear stress and strain amplitude. Many different materials follow the shear models, including aluminum alloys, steels, and superalloys. The majority of critical plane models have been developed in relation to the shear stress and strain components, trying to maximize a damage parameter related to a function of fatigue life in cycles. Under HCF conditions, the damage parameters are often computed using the normal and shear stress terms, since stress is related linearly to strain, and the stresses encountered are usually below the yield limit of the material. Under LCF conditions, damage parameters are typically computed using the normal and shear strain terms instead, since LCF conditions can exceed the yield limit of the material, creating a nonlinear relationship between stress and strain.

Overall, critical plane models have shown to be effective at fatigue life estimation. Numerous models have been proposed the last few decades, with the most common models examined in this section. The main drawback of critical plane models is the extra computational time required, as well as curve fitting for constants in some models.

The first well known critical plane model was proposed by Findley [21] during the 1950s. Findley developed the parameter based upon the shear stress amplitude and normal stress, with the critical plane being where the parameter was maximized. The equation below shows the Findley model, equated to a defined term of the fatigue life.

$$\left[\frac{\Delta\tau}{2} + k\sigma_n\right]_{max} = f(N_f) \tag{2.11}$$

$\Delta\tau$ is the shear stress range, σ_n is the normal stress, k is a material calculated constant, and $f(N_f)$ is a term that is a function of the fatigue life, all calculated on the critical plane where the

parameter is largest. Findley's parameter has shown promising data correlation in HCF situations [10], and is typically used for such cases.

Later in 1973, Brown and Miller [22] proposed that cracks initiate on planes of maximum shear strain, concluding that shear strain and normal strain were responsible for initiating cracks on the critical plane. The Brown-Miller parameter is shown below in equation 2.12.

$$\frac{\Delta\gamma_{max}}{2} + s\Delta\varepsilon_n = f(N_f) \tag{2.12}$$

$\Delta\gamma_{max}$ is the maximum shear strain range on the critical plane, $\Delta\varepsilon_n$ is the normal strain range on the critical plane, and s is a material-based constant. This criterion is more often used for LCF conditions since strain terms are used.

Commonly used today is the Fatemi-Socie model developed in the 1980s. Fatemi and Socie [23] proposed that the physical relationship for fatigue damage was based upon the maximum shear strain range, and the maximum normal stress on the critical plane throughout the loading cycle. Figure 2.1 illustrates the Fatemi-Socie model; as the shear strain amplitude increases, the cracks at the microscopic level begin to propagate, being resisted by frictional forces between the surfaces. The normal stresses on the critical plane promote the crack to grow, by separating the crack surfaces, reducing the frictional forces.

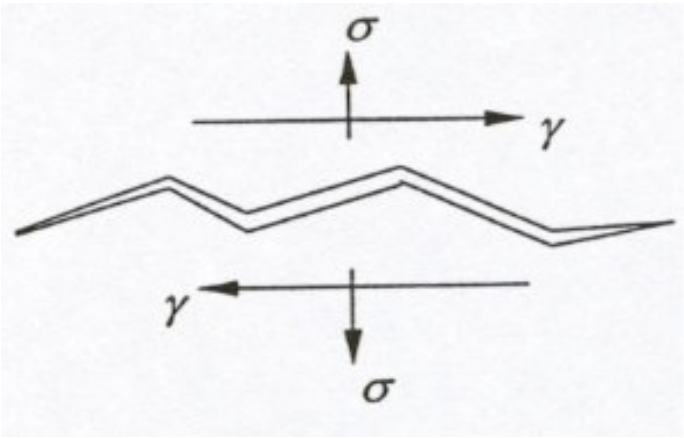

Figure 2.1. Illustration of the Fatemi-Socie model [23].

Equation 2.13 shows the Fatemi-Socie model, and its development in relationship to shear constants found from fully reversed torsion testing. The main advantage of the Fatemi-Socie model over other earlier critical plane models was the ability to account for mean stress effects.

$$\frac{\Delta\gamma_{max}}{2}\left(1 + k\frac{\sigma_{n,max}}{S_y}\right) = \frac{\tau_f'}{G}\left(2N_f\right)^{b_0} + \gamma_f'\left(2N_f\right)^{c_0} \tag{2.13}$$

$\sigma_{n,max}$ is the maximum normal stress on the critical plane, k is a material constant, S_y is the yield strength of the material, τ_f' is the shear fatigue strength coefficient, G is the shear modulus, γ_f' is the shear fatigue ductility coefficient, b_0 is the shear fatigue strength exponent, and c_0 is the shear fatigue ductility exponent. Research has shown that this parameter demonstrates great promise for data correlation of metallic materials [1, 14].

In the case of brittle materials, Socie [24] suggested a modification to the SWT parameter, with the intention of creating an effective tensile-based critical plane model. The new modified parameter was maximized based upon tensile stress and strain terms, which are more responsible for crack nucleation in brittle materials. The equation below replaces two terms on the left hand side of the SWT parameter with multiaxial equivalent terms.

$$\left(\sigma_{n,max}\frac{\Delta\varepsilon_1}{2}\right)_{max} = \frac{\sigma_f'^2}{E}\left(2N_f\right)^{2b} + \sigma_f'\varepsilon_f'\left(2N_f\right)^{b+c} \tag{2.14}$$

In this equation, $\Delta\varepsilon_1$ is the principal strain range.

Numerous critical plane models have been proposed, with the aforementioned models commonly accepted. Critical plane models predict multiaxial fatigue very well, due to their approach of physical observations of crack nucleation. Though mainly proposed to be used in multiaxial fatigue life estimation, the critical plane models can also be applied to uniaxial and

torsion loading scenarios. Many uniaxial loading circumstances naturally apply multiaxial stress states to materials, particularly when notches are present.

2.3. Notch Effects

Notches are a common occurrence in engineered components, whether holes for bolts to pass through, or notch roots to transition between parallel surfaces. Notches can create stress and strain concentrations in the local area. Stress gradients can also be introduced into the cross section of a component due to notch effects. These factors can greatly affect the fatigue life of a material, whether uniaxial or multiaxial. Most research in the last century sought to modify existing uniaxial fatigue theory, typically with a fatigue notch factor, K_f. Recently more research has been done in the area of multiaxial fatigue with notches in the material.

2.3.1. Uniaxial Notch Fatigue

Between 1950 and 1990, major theories guiding notch sensitivity in uniaxial notch fatigue were developed. Under HCF conditions, stress life approximations were developed by Neuber [25] and Peterson [26] to account for notch sensitivity. For LCF conditions, strain life approximations were more appropriate for calculating fatigue life. Neuber's [27], Glinka's [28], and the linear rule are the most common models, depending if the component induced plane stress, plane strain, or effects that fell in between. In 2011, research was done by Sakane et al. [13] to compare Neuber's rule against finite element analysis (FEA) to compare notch root stress predictions, with the FEA model underestimating crack initiation life, while Neuber's rule overestimated crack initiation life. The main drawback of the uniaxial notch fatigue modifications is their nature to modify existing uniaxial models, creating mostly scalar values. With notches, multiaxial stress states are almost always induced with axial loads; however, if multiaxial stress states are introduced directly to the notched component, the uniaxial theories for

notches do not provide sound fatigue life estimation. Some methods to adjust for notches in fatigue by developing a term to be used in uniaxial fatigue life equations have been developed.

A more recent method to compensate for fatigue in notches was proposed by Murthy et al. [29]. This method, called the stressed surface area approach, accounts for the stress gradient effect by considering the stress distribution on the surface of a component in the area close to the notch [30]. The basis of this method relies primarily on the concept of the "weakest link," where failure will initiate at a weak grain or defect in the material. If a small surface area is subjected to a stress, the probability of survival is expressed as equation 2.15 below. The probability is based upon a two-parameter Weibull distribution.

$$\left(R_0(\sigma_i)\right)^{\Delta A_i} = \left(\exp\left[-\left(\frac{\sigma_i}{\beta}\right)^{\alpha}\right]\right)^{\Delta A_i} \tag{2.15}$$

In equation 2.15, R is the probability of survival, σ_i is the stress, α is the shape factor, and β is the scale parameter. If the probability of survival for all areas were summed together, along with the assumption that two specimens will have the same probability of survival if at the same load, equation 2.16 below would result from these assumptions.

$$\Delta\sigma_{eq,1} = \left(\frac{Fs_2}{Fs_1}\right)^{1/\alpha} \Delta\sigma_{eq,2} \tag{2.16}$$

$\Delta\sigma_{eq,1}$ is the uniaxial equivalent stress range, $\Delta\sigma_{eq,2}$ is the equivalent stress range at the notch root, and Fs is defined by equation 2.17 below.

$$Fs_j = \sum_{i=1}^{n}\left[-\left(\frac{\sigma_{i,j}}{\sigma_{max,j}}\right)^{\alpha}\right]\Delta A_{i,j} \tag{2.17}$$

$\sigma_{max,j}$ is the maximum stress on the surface of the specimen, typically at the notch root, $\sigma_{i,j}$ is the stress at the particular area, $\Delta A_{i,j}$. For a given fatigue life calculation of a notched specimen, the uniaxial equivalent stress range term in equation 2.16 can then be used in equivalent stress fatigue life equations.

2.3.2. Multiaxial Notch Fatigue

Multiaxial fatigue modeling in notches currently has uncertainty in its direction. Current multiaxial fatigue models, such as critical plane models, can predict crack nucleation life fairly well due to their theoretical foundations built on physical characteristics of cracks. Stress gradients introduce more uncertainty into the analysis with respect to crack propagation life, but some research has shown that this can be accounted for in certain loading scenarios. Both HCF and LCF have been examined by researchers recently with respect to notches [12, 31, 32, 33]. The research area of multiaxial fatigue in notches is still in development, and is continuing to be explored as of present.

2.4. Biaxiality Ratio

The biaxiality ratio (BR) is typically defined as the ratio of the second principal stress over the first principal stress, shown in equation 2.18 below.

$$\lambda = \frac{\sigma_2}{\sigma_1} \tag{2.18}$$

$\sigma_{1,2}$ are the first and second principal stresses, respectively. For a basic tensile specimen, this ratio is typically zero, since there is no second principal stress present, even during fatigue loading. With the introduction of notches, such as a hole through a plate, this ratio begins to depart from zero. In plane stress scenarios, this ratio has a zero value on the surface, and a value close to zero moving away from the hole. In plane strain, this ratio, elastically and especially plastically, increases as the part is increased in thickness with respect to the notch root. Therefore, for a notched specimen that has the same layout on a plane with varying thickness, the stress gradient present from the notch will be the same between the different thicknesses. The main difference will be the BR, as the BR will normally increase in value as the thickness of the component increases, creating a plane strain situation.

The biaxiality of stress and strain in proportional loading has been examined in the past, with strong attention toward notches experiencing multiaxial stress states from uniaxial loading. Hoffman and Seeger [34] developed a method for estimating multiaxial stress and strain effects from the biaxial strain ratio. This research provided a theoretical extension to Neuber's rule, with particular attention to multiaxial stress and strain states in notched geometries. Work has also been done by Klann et al. [35], which sought to develop a multiaxial correction factor for uniaxial stress-strain curves of materials. This research showed strong correlation to common notch geometries. Research into the BR when using multiaxial fatigue criteria must be considered, since many multiaxial fatigue models develop constants separate from existing uniaxial fatigue models.

Uncertainty exists for which family of multiaxial fatigue models should be used with respect to the BR. For a given value of the first principal stress and a third principal stress of zero, if the BR falls between zero and one, especially around 0.5, a fatigue life benefit is generally calculated from equivalent stress/strain models because the magnitude of the equivalent stress/strain decreases. Conversely, many critical plane models are based upon the maximum shear stress/strain, which has no direct relationship to the BR. Due to this nature, many critical plane models are seen as Tresca theories, which are unaffected by the second principal stress and strain throughout the loading cycle. Therefore, if specimens of the same planar geometry exist, but with different thicknesses, equivalent stress/strain theories usually predict a life benefit for the thicker specimens, while the critical plane theories do not provide a clear life benefit, since the range between the first principal stress and third principal stresses is very similar between the thicknesses.

Previous work has examined effects of the biaxiality ratio in multiaxial fatigue. One of the earlier studies by Morrow and Kurath [36] suggested that appropriate multiaxial fatigue life models are material dependent, and the accuracy of different models will vary between different materials and microstructures.

Work done by Lefebvre [37] was aimed at examining the effect of triaxiality, and how it affects fatigue life for biaxial specimens. It was determined that critical plane parameters don't properly account for the secondary stress, or a change in the BR. Also, equivalent stress models with no adjustment for ductility reduction, brought on by a positive BR, can overestimate the actual fatigue life.

In 2009, Zhang [38] investigated the crack initiation of rig tests that included different biaxiality ratios throughout the structure. In essence, it was recognized that a debit factor for the life as a function of the biaxiality ratio was needed, and was applied to Sines' [15] formulation for an equivalent stress parameter. This research suggested that a positive BR can reduce LCF fatigue life due to lack of ductility.

Research was performed by Menton et al. [39] in predicting the minimum LCF life of scaled turbine minidisks. Despite the principal stress parameter in the study showed better correlation of the experimental data, it was determined that equivalent stress calculations needed to be corrected using the BR or similar stress ratios for better fatigue life estimation as well.

Based upon an initial review of literature, it is suspected that a possible life benefit exists for positive BRs. The focus of this thesis study is to determine if the BR provides a fatigue life benefit for specimens with varying BRs. Verification is performed using experimental data from notch specimens of different thicknesses.

3. BACKGROUND

The NDSU fatigue group has performed many different studies through the past 15 years. Much of this research has been dedicated to investigating new multiaxial fatigue critical plane parameters, particularly with high strength metals such as Ti-6Al-4V and nickel-based superalloys.

3.1. Previous Work

Previously, Kallmeyer et al. [10] examined many different equivalent stress and critical plane multiaxial fatigue models, evaluating their effectiveness against Ti-6Al-4V data from both uniaxial and biaxial testing. Overall, the Findley parameter, shown previously in equation 2.11, showed the best correlation, which is consistent with expectations due to the parameter showing strong correlation for high cycle fatigue (HCF) scenarios. Another critical plane model, the Fatemi-Socie parameter, in equation 2.13, and the Manson-McKnight equivalent stress model, also showed promise.

Later, Erickson et al. [17] examined the different variables with respect to crack nucleation in non-proportional loading. The new parameter developed showed promise and good correlation of results for the four materials examined, but the proposed parameter was stress-based, and it was noted that including strains may have a positive impact on fatigue life prediction, particularly in the area of low cycle fatigue (LCF).

To improve the previously proposed parameter, Feierabend [40] sought to include strain terms in the parameter as a technique to improve the parameter's correlation with LCF data in multiaxial fatigue life prediction. The result of the proposed strain-based parameter showed much better fatigue data correlation in the LCF regime, while adequately predicting transitional and HCF fatigue lives. This research provided a great starting point for the NDSU fatigue group

in developing critical plane models that mixed the effects of shear stress and strain as the primary driver for crack nucleation, with normal stress and strain providing a secondary influence.

3.2. Development of Current Damage Parameter

Throughout the past few years, the NDSU fatigue group has worked to develop a critical plane parameter that correlates well with data from various types of loading, including proportional and non-proportional load paths. A more recent critical plane parameter leading into this study is shown in equation 3.1 below, which is calculated on the plane of maximum shear strain amplitude.

$$DP_{old} = |\tau_{max}|^{1-w}(G\Delta\gamma_{max})^{w}\left(1 + k\frac{(\sigma|\tau|)_{max}}{\sigma_0^2}\right) \tag{3.1}$$

In this parameter, G is the shear modulus of the material, $\Delta\gamma$ is the shear strain range on the critical plane,τ_{max} is the maximum shear stress during the cycle on the critical plane, σ_0 is a unit conversion term, and $(\sigma|\tau|)_{max}$ is the value in which the product of the shear stress and normal stress is maximized throughout the cycle on the critical plane. The constants k and w are material constants fit from fatigue data. The constant w can be fit from torsion data at varying mean stress levels, as the constant k will drop out since normal stresses will not occur during torsion testing. The constant k can then be fit by including other types of loading, such as uniaxial, and biaxial test data. The stresses and strains to be used in equation 3.1 are calculated from techniques such as finite element analysis (FEA) using elastic-plastic behavior to account for residual stresses.

A major concern with equation 3.1 was the unit conversion term, σ_0. This failed to provide scalability of the shear stress during the loading cycle, and an adjustment was determined to be necessary for better data correlation. By replacing the unit conversion term with the maximum shear stress during the loading cycle, τ_{max}, an improvement in the overall fit to

the data was obtained. The final form of the damage parameter, DP, is shown in equation 3.2 below.

$$DP = |\tau_{max}|^{1-w}(G\Delta\gamma_{max})^{w}\left(1 + k\frac{(\sigma|\tau|)_{max}}{\tau_{max}^{2}}\right) \tag{3.2}$$

The new DP of equation 3.2 was compared against the old DP of equation 3.1 with previous experimental fatigue data. Figures 3.1 through 3.4 below show a comparison of the new DP versus DP_{old} using existing experimental uniaxial, torsion, and biaxial data from Ti-6Al-4V and DA 718. The computations for the stresses and strains were carried out in a similar manner as before, using the elastic-plastic behavior of materials. The proposed modification, which led to DP, effectively scaled the k term for different loading conditions. Fundamentally, Ti-6Al-4V and DA 718 are different in their material properties and microstructure, but the study performed previously by Krgo [9] showed that Ti-6Al-4V provided good correlation for critical plane models. Overall, the new DP provided a better and tighter correlation of existing fatigue data from different metals used in aircraft engine construction.

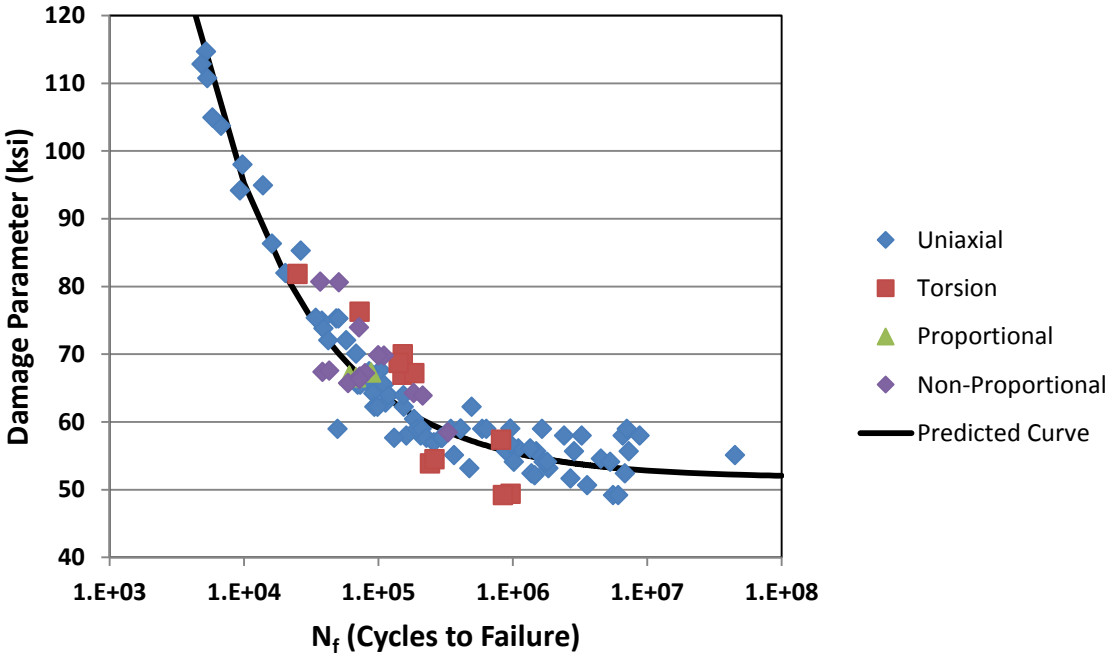

Figure 3.1. Correlation of Ti-6Al-4V data using new damage parameter (Eq. 3.2).

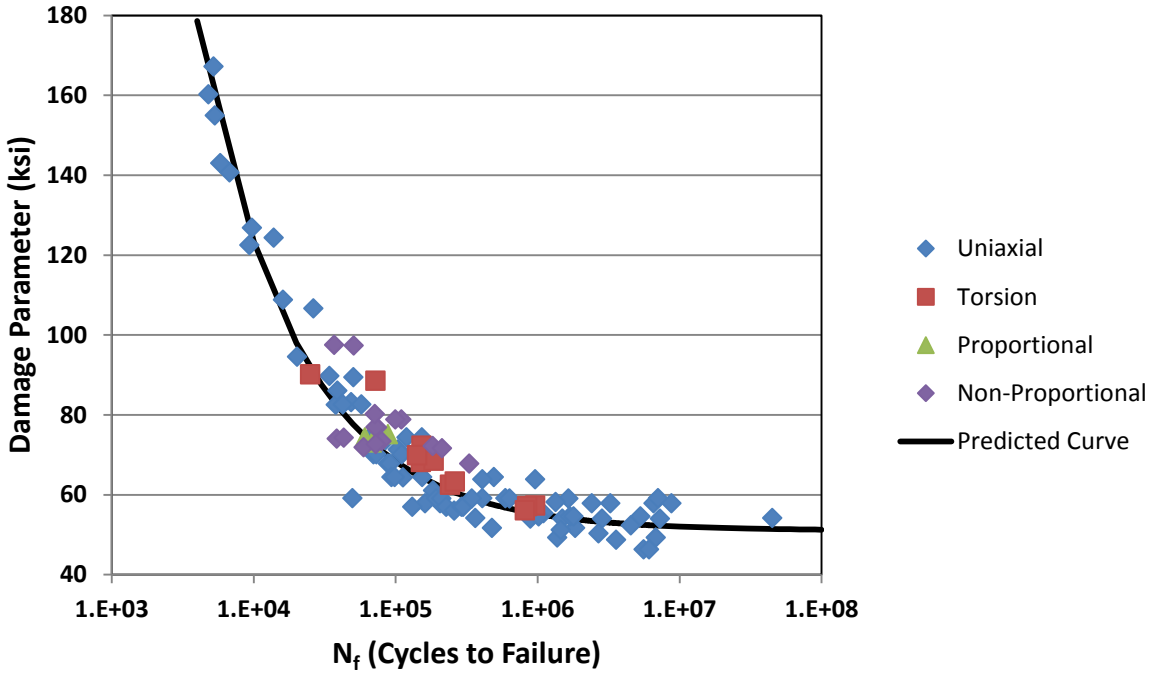

Figure 3.2. Correlation of Ti-6Al-4V data using old damage parameter (Eq. 3.1).

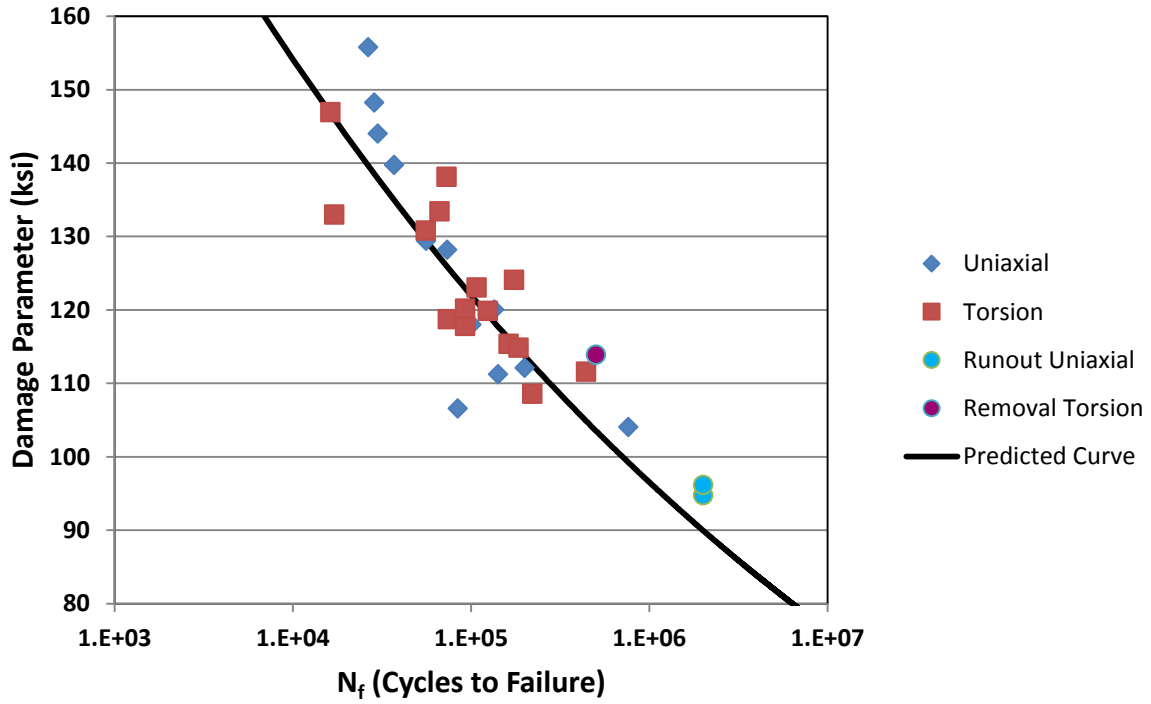

Figure 3.3. Correlation of DA 718 data at 75°F using new damage parameter (Eq. 3.2).

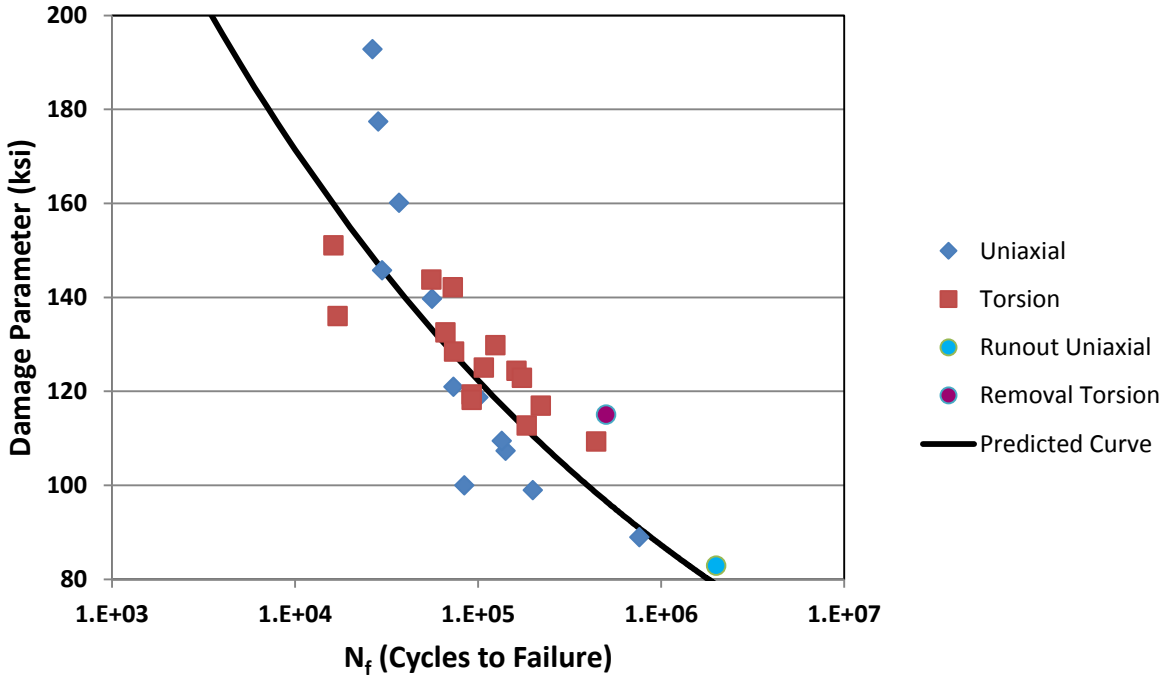

Figure 3.4. Correlation of DA 718 data at 75°F using old damage parameter (Eq. 3.1).

3.3. Analysis of Proposed Multiaxial Fatigue Models

3.3.1. Pseudo Stress Parameter

An existing equivalent stress model for multiaxial fatigue life prediction, known as the Pseudo Stress Parameter (PSP), uses the equivalent (von Mises) stress amplitude at the location where the equivalent stress is highest on the component in question. Knowing the R ratio of the loading, the equivalent stress amplitude at the critical point is input into a life prediction equation fit from experimental fatigue data at that R ratio. The PSP assumes complete elastic behavior as the material model for classical and finite element analysis (FEA). Equation 3.3 below shows the equation with the power law used to fit the constants for multiaxial fatigue life prediction.

$$PSP = \sigma_{eq,a} = P\left(N_f\right)^z \tag{3.3}$$

$\sigma_{eq,a}$ is the equivalent (von Mises) stress amplitude at the critical point in the component, N_f is the fatigue life to failure, and P and z are constants fit from experimental data.

The advantage of the PSP is the ease of its implementation. The equivalent stress is a scalar value, which allows for easy application, even in complex geometries. Research has also shown it to correlate to proportional loading fairly well [10]. However, several concerns are typically associated with equivalent stress models, including the PSP. The PSP cannot account for non-proportional loading effectively, and being a scalar value, it doesn't physically represent phenomena such as crack nucleation or crack growth.

3.3.2. Critical Plane Damage Parameter

The modified critical plane damage parameter, as shown in equation 3.2, is a new parameter proposed by NDSU for use in industrial applications. When fit to a power law equation for life prediction, the parameter takes the form as shown in equation 3.4 below. For most fatigue parameters, a double power law is more desirable due to the large range of fatigue lives, but since the range of this study was going to be small, a single power law was acceptable.

$$DP = |\tau_{max}|^{1-w}(G\Delta\gamma_{max})^{w}\left(1 + k\frac{(\sigma|\tau|)_{max}}{\tau_{max}^{2}}\right) = A\left(N_f\right)^{b} \tag{3.4}$$

A and b are experimentally fit constants from multiaxial fatigue data for each material. In application, different from the PSP, elastic-plastic material behavior is assumed in classical practice and FEA. This is to account for initial residual stress development, particularly in LCF situations. The model, as mentioned before, uses the input values at the plane of maximum shear strain amplitude.

By far the first major advantage of equation 3.4 is the inherent ability for it to account for non-proportional loading, a phenomenon that is often associated with critical plane models for multiaxial fatigue life prediction. The parameter also attempts to model the physical behavior of

cracks in metals, with shear stress and strain driving the initiation of cracks on the critical plane and normal stresses promoting the opening of cracks, similar to what Fatemi and Socie proposed in their model [23]. One disadvantage of the model, common with critical plane models in general, is the extra computations required to be carried out over the history of the stress and strain tensors to find the critical plane itself.

3.4. Biaxiality Ratio Effect

The biaxiality ratio (BR), as defined previously in equation 2.18, is the ratio of the second principal stress over the first principal stress, and can naturally fall between negative infinity and +1, depending on how low the third principal stress value is.

The BR has a strong influence when comparing the equivalent stress parameter (PSP) and critical plane parameter (DP) in fatigue life predictions, as shown as an example in figure 3.5 below. For figure 3.5, the first principal stress is held at 150 ksi, the third principal stress is held at 0 ksi, with the BR varying from zero to one. If the first and third principal stresses remain constant, and the BR increases from zero, the PSP, being an equivalent stress model, will naturally produce a fatigue life benefit, since the equivalent stress will decrease.

Conversely, the DP is more characteristic of a maximum shear stress/strain criterion (Tresca), meaning that the second principal stress is ignored for the fatigue life calculation. Therefore, as the BR departs from zero toward one, the DP is not affected in its fatigue life prediction, since the computed value will be the same despite a change in the BR.

This provides a design dilemma for engineers when computing multiaxial fatigue life. If the BR is positive, the PSP computes a longer fatigue life due to the lowering of the equivalent stress value, while the DP is not influenced by this occurrence. To date, little to no research has

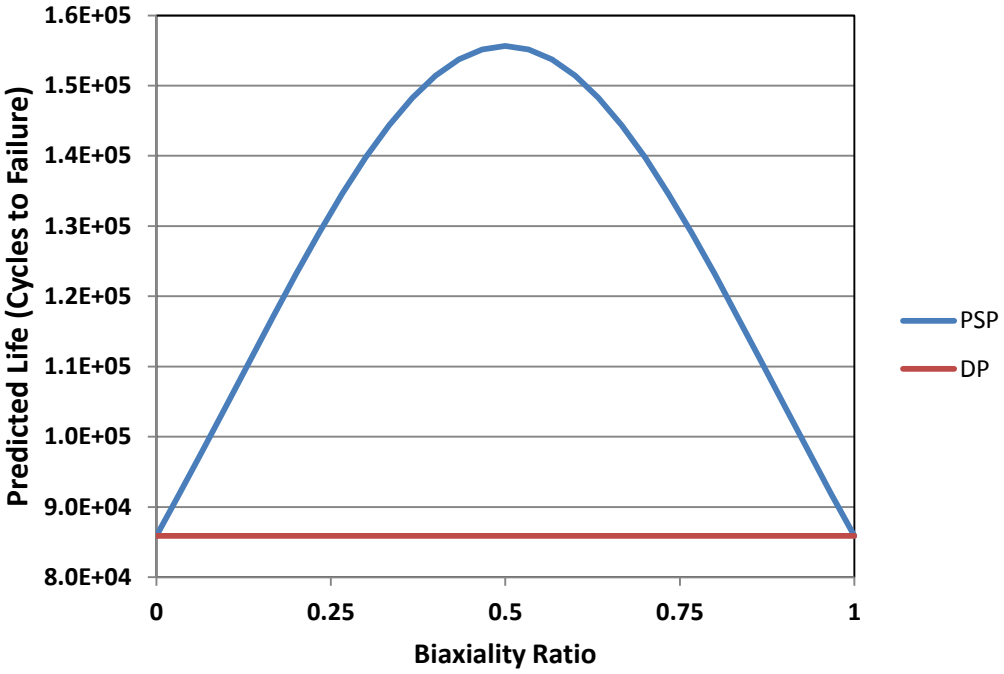

Figure 3.5. Biaxiality ratio influence on PSP and critical plane DP.

been found to directly investigate the effect of the BR on fatigue life. Thus, little data exists to verify which approach is more accurate in this scenario.

The purpose of this study is to investigate the influence of the BR on the fatigue life of metallic materials at room temperature. In order to directly study the effect of the BR, it was discerned that experimental testing must be performed on specimens that hold the first and third principal stress constant, but differ on the value of the second principal stress, inducing a positive BR. The PSP and DP are the two parameters that will be used for fatigue life estimation. If the BR does influence the fatigue life, adjustments to the DP will also be considered in this study.

4. SPECIMEN DESIGN AND DEVELOPMENT

4.1. Introduction

To investigate the influence of the BR, a suitable group of specimens needed to be designed that provided a significant difference in the BR value, without a significant change in the stress gradient or other characteristics between the specimens. Three types of specimens would be needed to evaluate the influence of the BR: a standard uniaxial LCF specimen to determine the material properties, and two specimens of similar geometry, but varying BR to evaluate the influence of the BR. The majority of this chapter is devoted to developing the two specimen designs that examine the BR influence.

Initially, the method of pressurizing a thin-walled cylindrical tube to produce a significant BR was considered, similar to the work performed by Morrow [14]. Equations 4.1 and 4.2 below are the formulations for the hoop stress and longitudinal stress for a thin-walled cylindrical tube, respectively.

$$\sigma_{hoop} = \frac{p_i r}{t} \tag{4.1}$$

$$\sigma_{long.} = \frac{p_i r}{2t} \tag{4.2}$$

For the above equations, p_i represents the internal, normal pressure in the tube, r is the internal radius, and t is the wall thickness. In the thin-walled assumption, the hoop, longitudinal, and radial stresses are considered the principal stresses with no shear components present. Since the radial stress is compressive, the BR for this system is the longitudinal stress over the hoop stress, which leads to a value of 0.5. As seen previously in figure 3.5, the PSP would predict a fatigue life benefit, while the DP would not be affected by the BR in its fatigue life prediction.

A pressurized thin-walled tube would provide an effective, direct method to examine the BR. This method encounters many difficult obstacles to overcome at the experimental level. First, a testing apparatus would have to be built to provide a strong, effective seal on the ends of the tube, which can be difficult to obtain. Due to the pressurization of the tube, the testing apparatus would have to be built in a safe location, since the pressurization and final rupture of a thin-walled tube would lead to a potentially strong decompression, introducing critical safety issues to the operator and other bystanders. After consideration, it was determined that other methods would be pursued.

The fatigue testing apparatus available at NDSU was an MTS servo-hydraulic axial load frame, with a rated fatigue load capacity of 50,000 lbs. Naturally the most effective method to examine the influence of the BR would be to use a load frame with biaxial loading capabilities. Due to the unavailability of such equipment, a specimen that could induce a BR on an axial load frame was ideal and necessary.

The MTS load frame's grips were another factor in choosing the size of the specimen. For cylindrical specimens, the vee grips have a maximum diameter capacity of 0.66 inches for side loading. Although the top loading maximum diameter capacity is one inch, the side loading constraint was used to keep the potential load levels down. For flat specimens, the flat wedge grips have a maximum size capacity of 0.67 inches. For very small specimens, shims can be used to close the grips onto the surface of the specimen.

Another consideration was material behavior when plasticity occurs. Since Poisson's ratio generally increases and approaches 0.5 with the onset of plasticity in metals, the BR would naturally increase as elastic-plastic deformation occurs. It was decided that the best approach was to use purely elastic values in the preliminary analysis to determine the optimal specimen design.

4.2. Specimen Design

Since the specimens would be used on an axial load frame, it was clear that a change in geometry was needed to induce a positive BR. Stress gradients are not desirable, but due to the nature of the study, stress gradients were a reasonable compromise. The stress gradients would have to be similar between specimens to truly study the effect of the BR. Some examples of geometry change include notches, grooves, bevels, and fillets. After an initial analysis, three geometries were primarily examined: a circumferential groove, a slot in the middle of a flat plate, and a hole in the middle of a flat plate.

Due to the complex geometry, the finite element analysis (FEA) solver ANSYS was used to examine the BR for in the three specimens. The R ratio is defined as the minimum load divided by the maximum load over the cycle, which is of importance when determining material properties. Different R ratios in the LCF region will produce different material properties. This study performs R = 0 loading cycles, in which the minimum load is zero.

The material properties used for the analysis were for DA 718 that were fit from previous experimental data at room temperature. The main analysis assumed elastic behavior, with elastic-plastic behavior examined further after the desired geometry was selected. Table 4.1 below contains the DA 718 material properties used in ANSYS for evaluating the three geometric designs. For plasticity, the model assumed multilinear kinematic hardening (MKH), developed from the experimentally fit Ramberg-Osgood coefficients for R = 0 loading at the half-life of the specimens.

The Ramberg-Osgood material model is displayed in equation 4.3 below. Usually equation 4.3 is used with the material's monotonic strain hardening coefficient and exponent. However, due to hardening or softening during cyclic loading, the cyclic properties for R = 0 are

Table 4.1. Direct Age 718 Material Properties for ANSYS Specimen Study (R = 0)

Property	Value
Elastic Modulus (E)	30,200 ksi
Poisson's Ratio (υ)	0.311
Cyclic Strain Hardening Coefficient (K')	285 ksi
Cyclic Strain Hardening Exponent (n')	0.0574
Cyclic Yield Strength (σ_y')	161 ksi
Ultimate Strength (σ_{ut})	260 ksi

more appropriate for the material model in this study. In equation 4.3, ε is the true strain, and σ is the true stress.

$$\varepsilon = \varepsilon_{elastic} + \varepsilon_{plastic} = \frac{\sigma}{E} + \left(\frac{\sigma}{K'}\right)^{1/n'} \tag{4.3}$$

4.2.1. Circumferential Groove

The circumferential groove consists of a semi-circle cut into a cylindrical shaft. The shaft is loaded in the axial direction, creating a stress concentration throughout the groove. Figure 4.1 shows a cross section of the circumferential groove. The dimensions of interest for the circumferential groove are the major diameter of the shaft, and the radius of the groove.

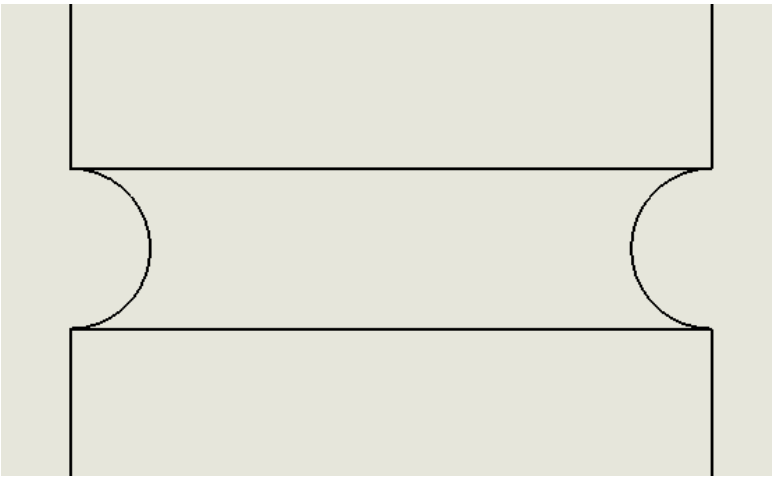

Figure 4.1. Cross section of circumferential groove.

For sizing, the ratio of the radius to the diameter was of importance. If the radius was too small, the groove would need to be treated like a fracture mechanics problem. Conversely, if the radius was too large, the net section stress would become very high, which was undesirable for this study. Another obstacle for this geometry is the stress gradient; it was unclear how to replicate a similar stress gradient, while inducing a change of the BR.

An FEA model of the circumferential groove was constructed to check the BR at the root of the groove. Figure 4.2 shows the ANSYS Mechanical mesh with quadratic elements, which was an axisymmetric model to lower the element count, thus increasing simulation speed. The boundary conditions for the model had the bottom edge fixed, with the load being applied at the top in the axial direction. The model assumed a major diameter of one inch, with a groove radius of 0.125 inches, reducing the radius to major diameter ratio, r/d, to 0.125. This ratio was considered the lower limit to avoid fracture mechanics behavior.

An elastic load of 1,000 lbs was applied axially to the model, which resulted in a BR at the groove root of 0.24. The model was checked for plasticity at that load level, and it was found that none occurred. Even though the ideal value of the BR would be around 0.5, 0.24 would be significant enough to contribute a noticeable life benefit to the PSP, while not adding a life benefit to the DP. It was also found that increasing the groove radius would drive the BR down toward zero, an undesirable effect.

After careful consideration, this geometry was not chosen mainly due to the inability to reproduce the stress gradient with different BR values. It was clear after this investigation that flat plate specimens would be more desirable, as cylindrical specimens would not provide an adequate way to introduce changes in the BR without major changes in the stress gradient.

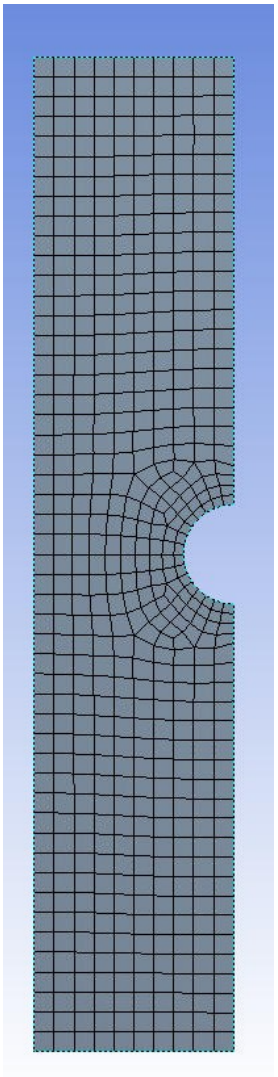

Figure 4.2. ANSYS axisymmetric mesh of circumferential groove.

4.2.2. Plate with Slot

Another geometry that was considered was a flat plate with a slot. The basic slot geometry is shown in figure 4.3 below.

In the case of the slot, four dimensions could generally be modified to influence the actual BR value: the plate width, the plate thickness, the slot height, and the slot width. The more critical aspects of the dimensions are the slot height, and the ratio of the slot width to the plate

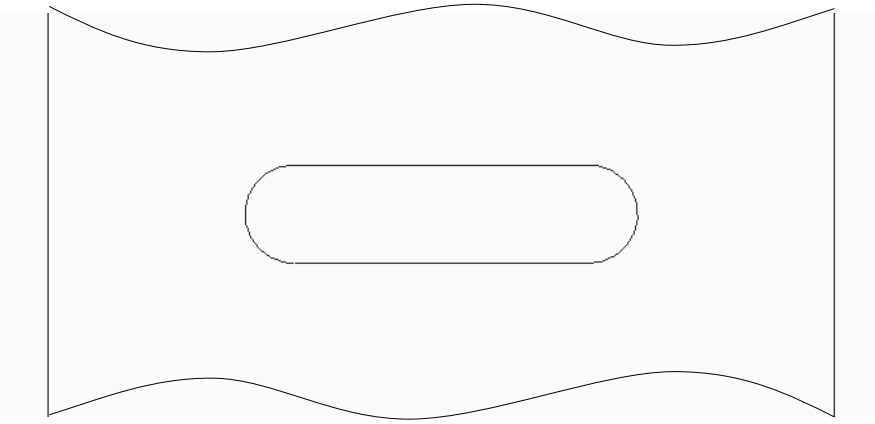

Figure 4.3. Cross section of a plate with a slot.

width. If the slot height is too small, the geometry more represents a crack with a fracture mechanics approach, similar to the circumferential groove. If the slot width is too large, the net sections stress would increase drastically, and would most likely produce unreliable, inconsistent experimental data.

An eighth symmetry ANSYS model was created to examine the BR at the root of the notch. For the model, the slot height was 0.125 inches, the total slot width was 0.5 inches, the plate width was one inch, and the plate thickness was 0.6 inches. The boundary conditions were three symmetric planes to constrain the model in all three directions, and the load was applied at the top of the model. Figure 4.4 below shows the swept mesh in ANSYS, using the eighth symmetry to simplify the model.

An elastic load of 4,000 lbs was applied to the model, which yielded a BR of 0.26. This was better than the circumferential groove, and would provide the ideal effects when comparing the PSP and the DP. However, due to the abnormal geometry, the manufacturing process of this specimen would be time consuming, as well as very expensive. Due to these factors, this specimen geometry was not chosen for this study.

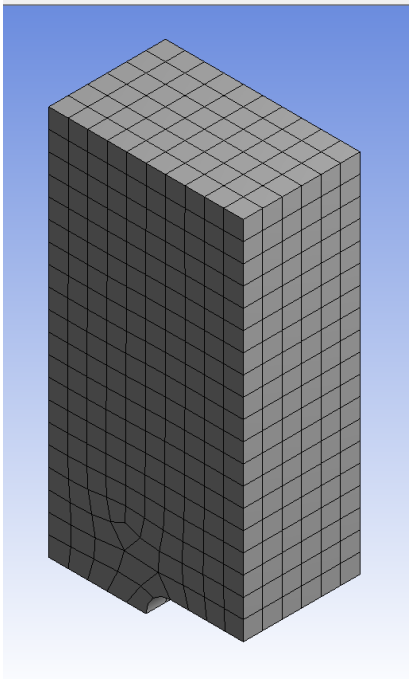

Figure 4.4. ANSYS eighth symmetry mesh of a plate with a slot.

4.2.3. Plate with Hole

Lastly, the geometry of a plate with a hole in the middle was examined, shown in figure 4.5 below. The three main dimensions that can be controlled to influence the BR are the plate width, the hole diameter, and the plate thickness. If the hole diameter is too small in relation to the plate width, manufacture of the specimen would become more difficult due to it being harder to apply the honing process on a smaller scale. On the other hand, if the hole diameter is too large, the net section stress would increase immensely, an undesirable trait.

As with the plate with a slot, an eighth symmetry model in ANSYS was created to study the BR. For the model, the plate width was set at 0.65 inches, the thickness to 0.6 inches, and the hole diameter at 0.25 inches. The boundary conditions are very similar to the plate with a slot, as three symmetrical planes are used, with the load applied at the top of the model. Figure 4.6 below shows the mesh used in ANSYS.

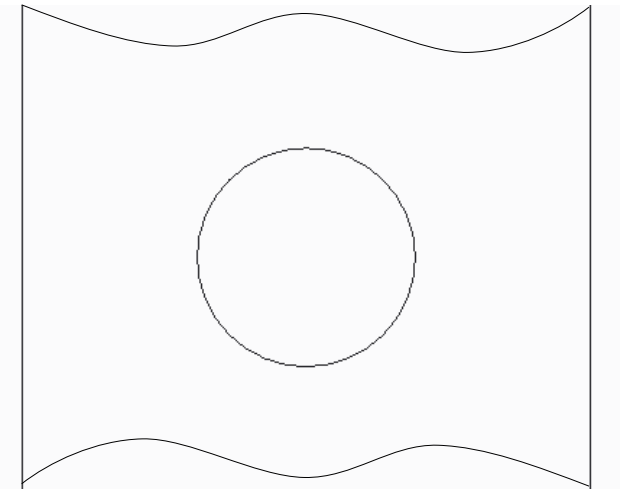

Figure 4.5. Cross section of a plate with a hole.

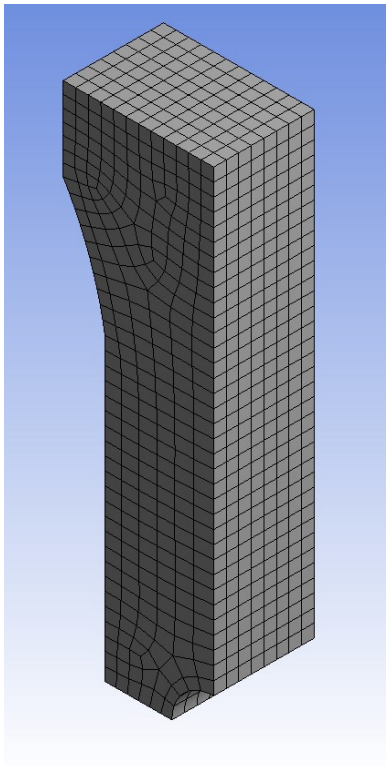

Figure 4.6. ANSYS eighth symmetry mesh of a plate with a hole.

An elastic load of 4,000 lbs was applied to the model, which yielded a BR of 0.22 at the notch root. This was an optimal value to compare the PSP and the DP while allowing control

over the stress gradient. Due to its simplicity, and being easily manufactured, the plate with a hole geometry was chosen to test the influence of the BR in this study.

4.3. Specimen Development

With the selection of the plate with a hole, the relationship between the hole diameter, the plate width, and the plate thickness was of great interest. As the plate becomes thinner, the geometry becomes more characteristic of a plane stress state, while as the plate becomes thicker, the geometry becomes more characteristic of a plane strain state. It was expected that as the thickness of the plate was decreased, the BR would decrease to zero at the edge of the hole, while as the thickness increased, the BR would increase.

4.3.1. Optimization

The ANSYS Goal Driven Optimization tool was utilized to find the right balance of manufacturing ease, while driving the BR up toward 0.5. Particular attention was given to the hole diameter, with the aim of using a diameter common in manufacturing. The optimization was more concentrated on determining the thick specimen dimensions, and maximizing the BR of the geometry. As with the other models, the DA 718 material model from table 4.1 was utilized. The maximum grip dimensions were taken into consideration when selecting the best dimensions for the thick geometry as well.

After the optimization procedure, the final dimensions for the cross section were chosen, shown in table 4.2 below, along with the calculated BR values at the notch root for elastic conditions. The main difference between the thin and thick specimen was the plate thickness. The hole diameter and plate width were kept constant to produce the same stress gradient for both the thin and thick specimen design.

Table 4.2. Specimen Design Dimensions

Specimen	Hole Diameter (in)	Plate Width (in)	Plate Thickness (in)	λ
Thin	0.25	0.65	0.1	0.034
Thick	0.25	0.65	0.6	0.201

The thin plate thickness of 0.1 inches was selected due to its common size without making it too thin for adequate gripping in the MTS load frame. The optimization process did not show any strong reduction of the BR by increasing or decreasing the thickness from 0.1 inches.

A plate thickness of 0.6 inches was chosen for the thick specimen because it fell within the maximum flat plate grip size. Also, the optimization process suggested that no significant increase in the BR was gained by increasing or decreasing the thickness from this value.

Figures 4.7 and 4.8 show the equivalent stress (von Mises) distribution of the ANSYS models for the thin and thick geometries, respectively. The loads for these figures were for the same net section stress in the axial direction of 16.67 ksi, which is vertical in these layouts and well below the yield strength of DA 718, even at the notch root. The meshes for both the thin and thick geometry were refined and modified for more accuracy.

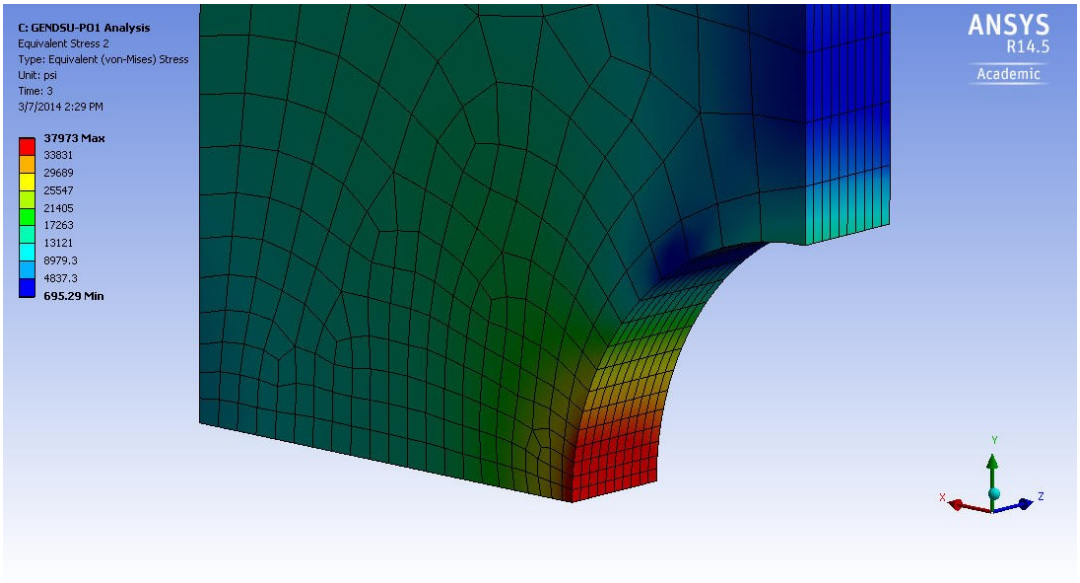

Figure 4.7. ANSYS equivalent stress distribution for thin geometry.

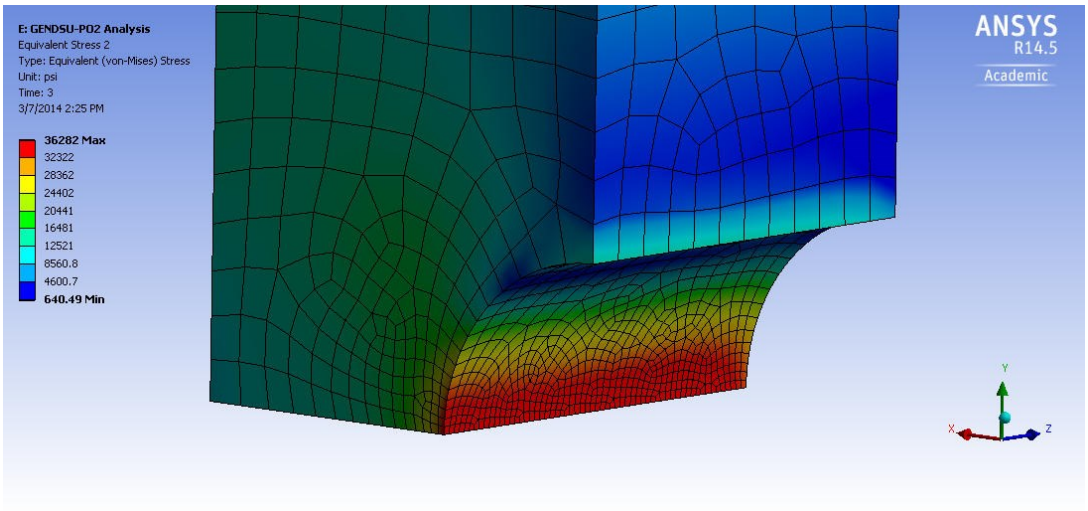

Figure 4.8. ANSYS equivalent stress distribution for thick geometry.

4.3.2. Finite Element Model Validation

To validate the BR from the ANSYS models, another FEA solver, PTC Creo Simulate 2.0, was used to validate the thick specimen value of 0.201. To better validate the model, the boundary conditions and loads that were applied to the original ANSYS model must be understood.

The analysis uses an eighth symmetry model, which was used to keep the node and element count down. The intent of using three symmetric planes was to increase the speed of the solution time, particularly if elastic-plastic deformation occurred in the model. A flat plate with a hole in the middle naturally has three planes of symmetry, all intersecting the middle of the hole. For symmetric boundaries, the displacement in the direction normal to the plane is fixed. The load is then applied on the top face, which is one quarter of the total load a full model would experience.

Using this concept, other models in other FEA solvers could be used to check the BR at the notch root. Figure 4.9 below shows the PTC model using eighth symmetry with the first principal stresses highlighted throughout the body. The final value of the BR for this PTC mesh was approximately 0.201 at the notch root with a load of 4,000 lbs. This was consistent with the ANSYS Mechanical calculated value for the BR, therefore the model was considered adequate and valid. The PTC model aided in verifying the validity of the ANSYS models used.

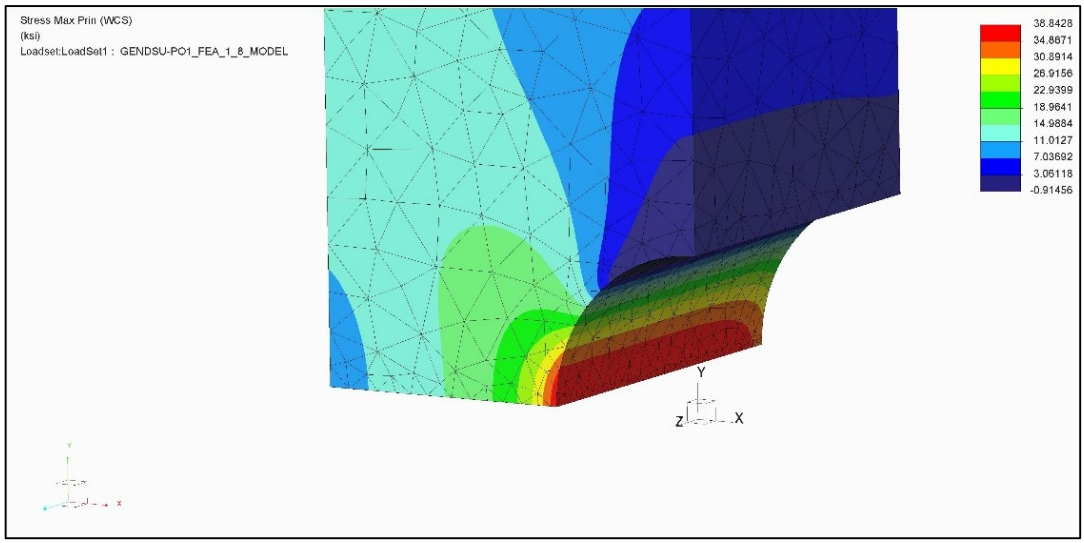

Figure 4.9. PTC Creo Simulate eighth symmetry model.

4.3.3. Final Design and Manufacture

For this study, a total of three specimens needed to be designed to evaluate the influence of the BR. The first design would have to be an LCF cylindrical specimen to obtain the material properties for the FEA solver, and for the fatigue constants in the PSP and the DP. The second and third designs would be the notched specimens used to evaluate the BR. In the case of the main cross section of the specimens, the dimensions were listed previously in table 4.2.

The surface finish is critical in fatigue specimen manufacturing, as any imperfections can lead to undesired crack initiation sites. Therefore, a very smooth surface finish tolerance was used in the manufacturing process, as well as chamfers at the ends of the notches, with the assumption that cracks will initiate at the notch root of the specimens.

For this study, two forgings of DA 718 were available for the manufacture of the specimens. The main objective for the final specimen designs was to prepare enough specimens to confidently examine the BR influence, without sacrificing too much grip area for the MTS load frame. After evaluation, a total of eight LCF specimens, eleven thin specimens, and eleven thick specimens were produced with the final dimensions shown in figures 4.10 through 4.12 below. Figure 4.13 shows the cutting pattern that was used on the two forgings of DA 718.

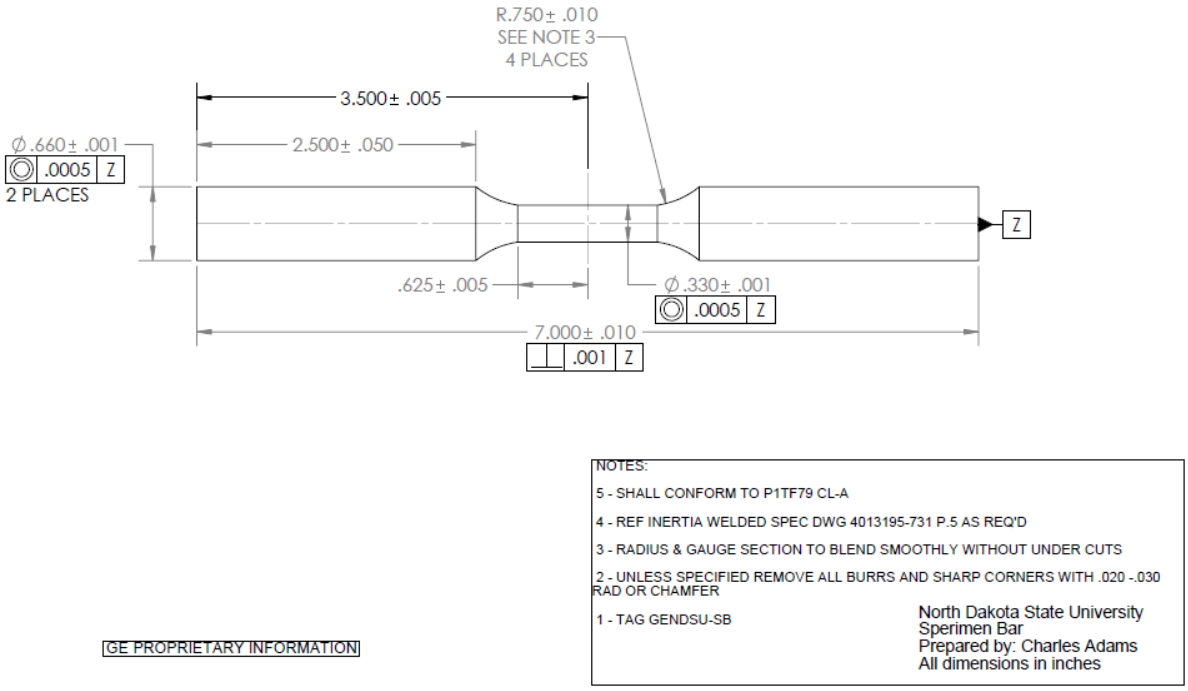

Figure 4.10. Dimensions of the GENDSU-SB LCF specimen.

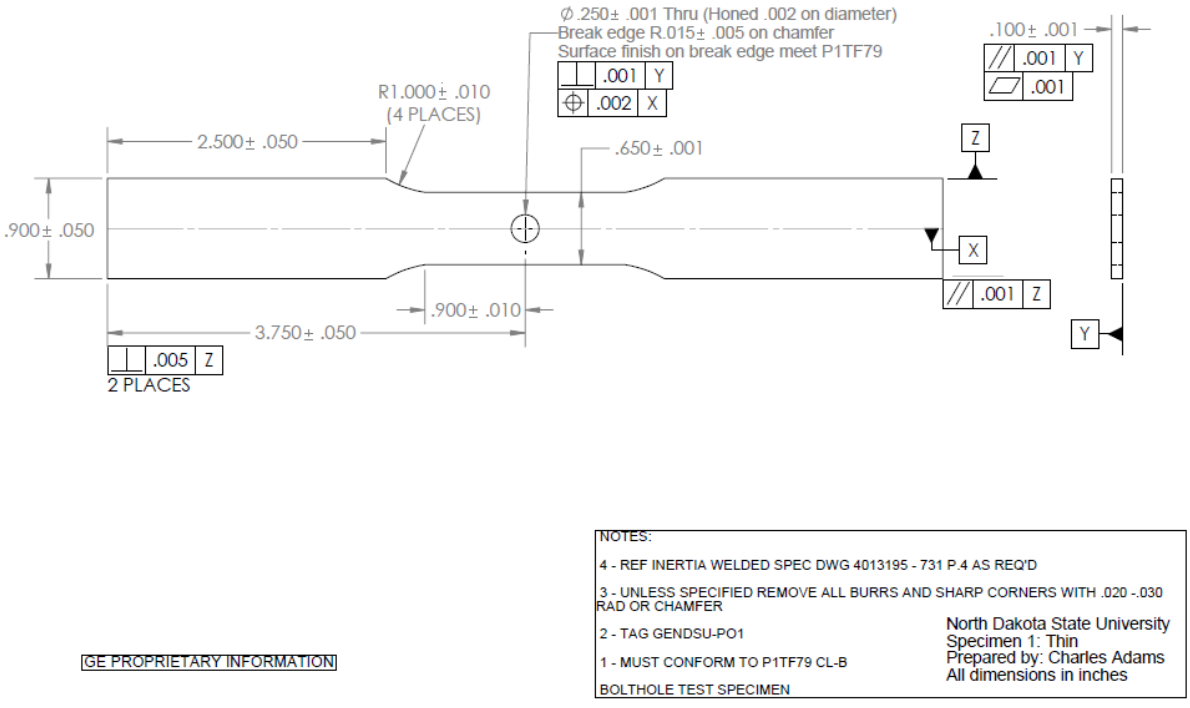

Figure 4.11. Dimensions of the GENDSU-PO1 thin specimen.

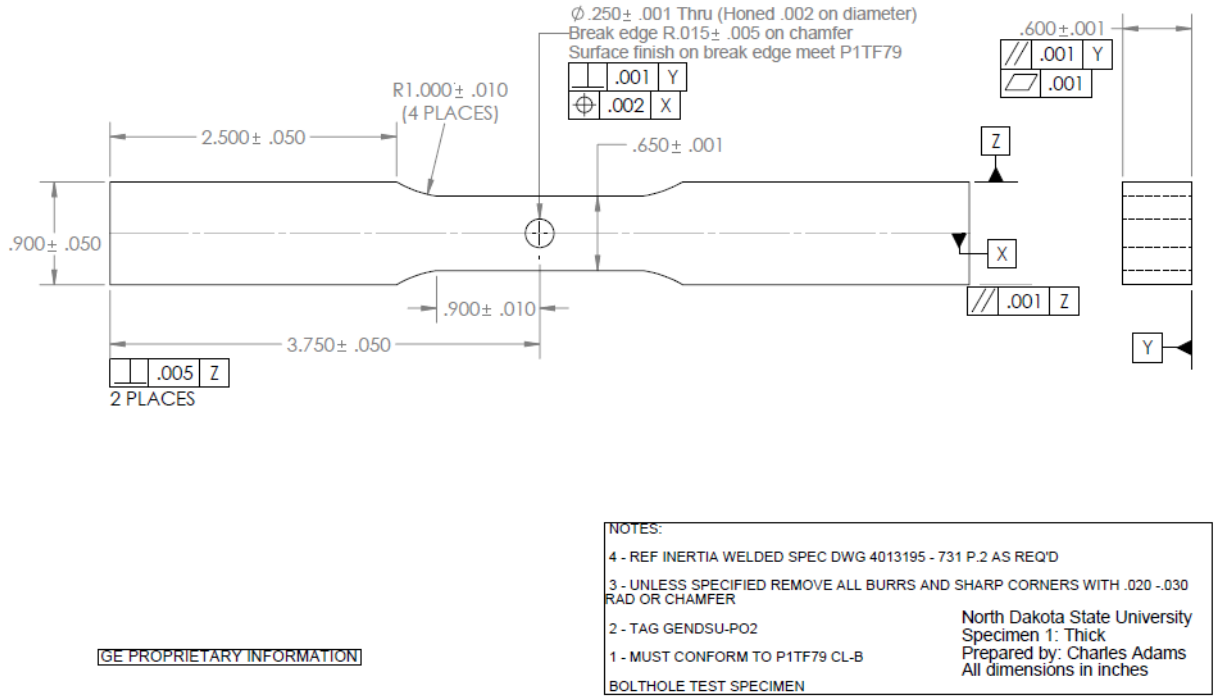

Figure 4.12. Dimensions of the GENDSU-PO2 thick specimen.

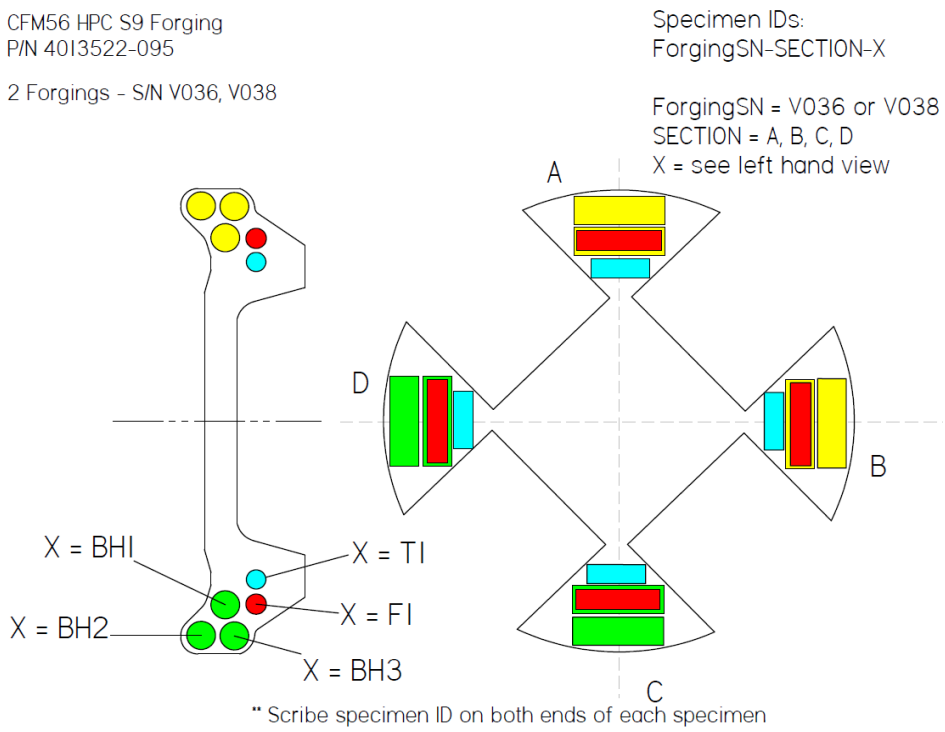

Figure 4.13. Cut pattern for the two forgings.

5. MATERIAL AND METHODS

This chapter discusses the material, testing equipment, and details of the experimental procedures used to evaluate the influence of the BR.

5.1. Material and Equipment

5.1.1. Material

Direct Age 718 (DA 718) is a nickel-based superalloy derived from wrought Alloy 718. DA 718 derives its properties of high tensile strength with fatigue resilience from its high forge reductions at low temperatures, and using an age only heat treatment [41]. This particular metal has seen much use in gas turbine disks for aircraft engines due to its high fatigue resistance combined with its high tensile strength. The general chemical composition of DA 718 is shown in table 5.1 below, showing the alloy and amount by weight percentage. The microstructure of the material is composed mainly of gamma phase matrix with small amounts of delta phase precipitates, TiN nitrides, and NbC carbides [41].

Table 5.1. DA 718 Approximate Chemical Composition [41]

Alloy Material	Weight %
Nickel	53.4
Iron	18.6
Chromium	17.9
Niobium + Tantalum	5.22
Molybdenum	2.95
Titanium	0.91
Aluminum	0.48
Carbon	0.04
Boron	0.003

5.1.2. Equipment

The testing apparatus used for this study was an MTS servo-hydraulic load frame with a rated fatigue load capacity of 50,000 lbs. The machine is capable of operating in stroke control, load control, and strain control.

Before any testing for the study occurred, the grips were checked for proper alignment per ASTM standard E1012. Bending loads due to machine misalignment could adversely affect the results for this study; therefore careful consideration was taken to verify the alignment of the load frame. A W2 tool steel dog bone dummy specimen was machined and heat treated to match or exceed the yield strength of previous DA 718 specimens. Eight strain gages were attached to the specimen, with four above the mid plane of the specimen equally spaced around the diameter, and four below the mid plane equally spaced around the diameter. The load frame was checked for alignment by loading the alignment specimen in four configurations 90° apart from each other. After collecting the strain gage data, the machine was considered suitable and aligned properly.

5.2. Methods

To effectively study the effect of the BR, a joint experimental-theoretical method needed to be developed for the three specimens, and the theoretical multiaxial fatigue parameters, the PSP and the DP. The method needed to relate the results of the strain-controlled LCF specimen design, GENDSU-SB, and the results of the two load-controlled notch specimen designs, GENDSU-PO1 (thin) and GENDSU-PO2 (thick).

5.2.1. LCF Specimen Methods

Since the material properties of DA 718 can change significantly enough between different forgings, LCF testing is used to develop and calculate the desired material properties.

For this study, eight LCF specimens were available, four from each of the two forgings. The LCF specimens were tested in R = 0 loading, with a minimum strain level of zero, and a predetermined maximum strain level. The strain levels that are chosen generally to exceed the yield strength to account for cyclic hardening and/or softening during the fatigue life of the specimen.

The material properties of interest were the elastic modulus, E, the cyclic strain hardening coefficient, K', and the cyclic strain hardening exponent, n'. After the material properties were calculated, the strain life fatigue constants for the DP and PSP could then be fit from experimental data. To aid in the development of these properties, the MTS load frame was used combined with a one inch gage length extensometer to run the tests in strain-control. Figure 5.1 shows the MTS load frame set up for the LCF specimens.

After the maximum strain value for the cyclic loading is selected, data collection is implemented for the cycle count, measured strain, and measured load. The first few cycles, typically around ten, are collected at a sample frequency that outputs close to 50 points per cycle. Throughout the testing, the peak and valley data are also collected until failure, as well as full cycles in a logarithmic sampling pattern, with four cycles per logarithmic decade of cycles. This allows for the data collection of the cyclic behavior at the startup of the procedure, the tracking of the maximum and minimum load values over the life of the specimen, and the examination of the cyclic behavior throughout the fatigue life.

With eight specimens available for R = 0 loading, tested at varying maximum strain levels, the plastic strain component of the Ramberg-Osgood equation can be rearranged, shown in equation 5.1, to fit K' and n' using a least-squares fit, seen in equation 5.2, by using software such as Microsoft Excel.

Figure 5.1. MTS load frame with a LCF specimen installed.

$$\sigma = K'\left(\varepsilon_{plastic}\right)^{n'} \tag{5.1}$$

$$LCF\ Least\ Squares\ Fit = \sum^{Specimen\ Count}\left[\frac{\left(\sigma_{exp}-\sigma_{theory}\right)}{\sigma_{exp}}\right]^2 \tag{5.2}$$

For equation 5.1, σ is the maximum true stress at the half-life of the specimen, and $\varepsilon_{plastic}$ is the true plastic strain at the maximum strain level at the half-life of the specimen. For equation 5.2, σ_{exp} is the measured maximum true stress value at the half-life of the specimen, and σ_{theory} is the predicted maximum true stress value at the half-life of a specimen using the Ramberg-

Osgood constants. Minimization of equation 5.2 is desired to closely fit K' and n' from the experimental results.

It is recognized that only eight specimens are available for developing the Ramberg-Osgood constants. In practice, more LCF specimens would be needed to develop more accurate and proper constants. However, the budget and material constraints of the study allowed for only eight LCF specimens in total. It is noted that the objective of the study is to evaluate the influence of the BR, not necessarily develop an accurate material model. Therefore, eight specimens were considered adequate for this study in developing a basic material model.

Once the material properties are determined, the material model is then transferred into ANSYS, using multilinear kinematic hardening (MKH) for the plasticity model. The MKH model is common for ductile metals, and has been proven to express plasticity behavior well in experimental testing. This material model can then be used in ANSYS to calculate the stresses and strains of complex geometries that undergo elastic-plastic deformation, particularly of the two notch specimens, GENDSU-PO1 and GENDSU-PO2.

After the material model is constructed, the fatigue constants for the PSP and the DP need to be fit using their corresponding calculated values and their fatigue lives. The PSP, in equation 3.3, follows a single power law relationship for the fatigue life in this study. Only two constants, P and z, need to be fit from the experimental data of the LCF specimens. To accomplish this, the calculated PSP for each specimen and its corresponding experimental fatigue life are used with a least-squares fit model in Microsoft Excel, shown in equation 5.3 below. As with the Ramberg-Osgood fit procedure, many more specimens would be needed to accurately fit the PSP constants, but the interest of the study is the BR influence, not how accurate the multiaxial fatigue models are in predicting the experimental fatigue life.

$$PSP\ Least\ Squares\ Fit = \sum^{Specimen\ Count}\left[\frac{(PSP_{exp}-PSP_{theory})}{PSP_{exp}}\right]^2 \quad (5.3)$$

PSP_{exp} is the PSP value from experimental calculations, and PSP_{theory} is the PSP value from the power law with the corresponding fatigue life. The goal is to minimize the value of equation 5.3 for a strong curve fit.

The DP constants can also be fit using the experimental fatigue lives of the LCF specimens, and their corresponding DP calculations. In equation 3.4, six constants in total are used to fit the equation with experimental data for this study. With only eight specimens, that does not provide a basic starting point to fit the constants while being highly accurate. If a reduction in the number of constants can be performed, this would aid in simplifying the curve fit procedure. The constants k and w are used to describe the DP from a solid mechanics standpoint, and are assumed to remain relatively unchanged between different forgings of DA 718. Therefore, previous experimental data can be used to fit k and w, which can then be kept constant when determining the fatigue life constants A, and b. The fatigue life term of equation 3.4 follows a power law, which can then be fit using the calculated DP for each specimen, with their corresponding experimental fatigue lives, shown in equation 5.4 below, using Microsoft Excel.

$$DP\ Least\ Squares\ Fit = \sum^{Specimen\ Count}\left[\frac{(DP_{exp}-DP_{theory})}{DP_{exp}}\right]^2 \quad (5.4)$$

For equation 5.4, DP_{exp} is the experimentally calculated DP, and DP_{theory} is the multiaxial fatigue life DP calculated from the power law equation. The goal is to minimize the value of equation 5.4, providing a strong fit between experimental data and the theoretical DP model.

Eight specimens would not be considered enough to develop an accurate multiaxial fatigue life model. However, eight specimens should be adequate to develop a general model comparing the thin and thick specimens and their fatigue lives relative to each other.

5.2.2. Notch Specimen Methods

Once the material model, PSP constants, and DP constants have been determined, the two sets of notch specimens can be tested. Using the material model developed previously in the LCF methods section, ANSYS is used to model the two specimens, determining the stresses and strains at the notch root. Using the stresses and strains at the notch root, the PSP and the DP can be calculated at a particular load level, with the assumption of R = 0 load control cycling at room temperature.

To determine the theoretical fatigue life estimation for the notched specimens at a given load level, ANSYS Mechanical models were constructed for both specimen designs. In the elastic analysis for the PSP, only one load step is necessary because no plasticity occurs in the model, meaning no residual stresses are present even if the yield strength of the material is exceeded. In the elastic-plastic analysis for the DP, four load steps total, representing two complete loading cycles, are needed in conjunction with the MKH model. If plasticity occurs, residual stresses will be present, affecting the stress and strain values at the maximum and minimum loads. When performing the theoretical DP calculation, the maximum load value at load step three and minimum load value at load step four (second cycle) are used to account for the initial plasticity that occurs with the first ramp up and ramp down (first cycle). Combined with the cyclic, R = 0 Ramberg-Osgood model used for the MKH model, the theoretical FEA model for the DP attempts to estimate the plasticity at the half-life of the specimen, while accounting for the plasticity that has already occurred over the fatigue life.

To accurately evaluate the influence of the BR, the load levels should be chosen so that the thin and thick notch specimens, GENDSU-PO1 and GENDSU-PO2, respectively, have the same net section stress value at the maximum load. From a preliminary analysis, the DP values for the same net section stress are very close together, suggesting that the specimens have virtually the same theoretical fatigue life according to the critical plane theory.

Two FEA models for the thin and thick notch specimens were constructed in ANSYS for the theoretical stress and strain calculations. For simplification, the three symmetrical planes were used as boundary conditions to create an eighth symmetry model, similar to the preliminary models developed in chapter four. The sweep meshing technique was utilized for uniform element placement, with line sizing for a finer mesh at the notch root. Quadratic brick elements were used, keeping the midside nodes for better accuracy.

Figure 5.2 below shows the thin notch specimen mesh in ANSYS. For this mesh, a total of 20,668 nodes are present, with a total of 4,370 elements. The load is applied at the top of the mesh in the vertical, axial direction. When a total load is used, the force on the model will be one quarter of the load due to the symmetric boundary conditions.

Figure 5.3 below shows the thick notch specimen mesh in ANSYS. For this mesh, a total of 34,833 nodes are present, with a total element count of 8,635. As with the thin specimen mesh, the load is applied at the top in the vertical direction, with the load applied on the model a quarter of the total load determined for the full specimen.

The stresses and strains at the notch root are used to calculate the PSP and DP. Since a stress gradient exists in these notch specimens, a knockdown factor must be used to approximate the true PSP and DP for the calculated fatigue life. In notched specimens, using the notch root stresses and strains for fatigue life prediction will typically result in an underestimated fatigue

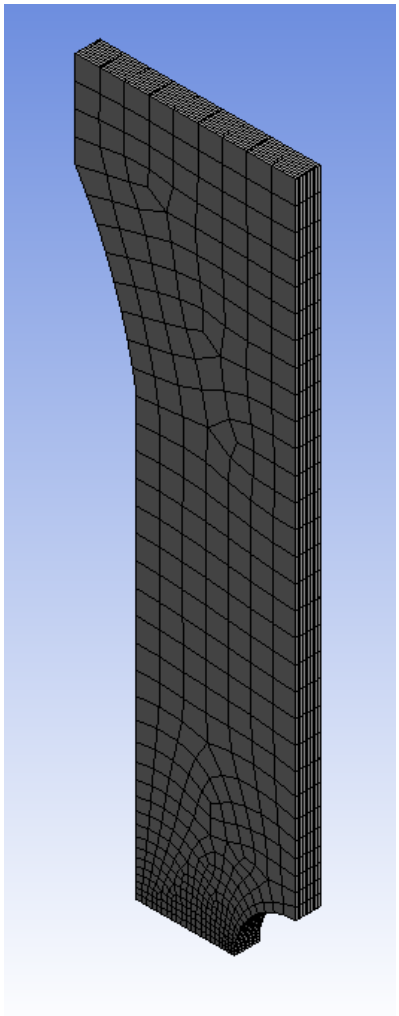

Figure 5.2. ANSYS eighth symmetry mesh of the thin notch specimen.

life compared with uniaxial, smooth specimens for the same stress and strain levels. This effect is due mainly to the stress gradient, which is not uniform throughout the specimen, creating high stresses on smaller volumes of the specimen, while inducing lower stresses on other volumes of the specimen. Therefore, the high stress levels at not uniform throughout the thickness of the specimen, statistically lowering the change of crack initiation.

In notched specimens subjected to uniaxial loading, a reduction from the calculated peak stress and strain values must be used to compensate for the notch gradient effect. One of the most

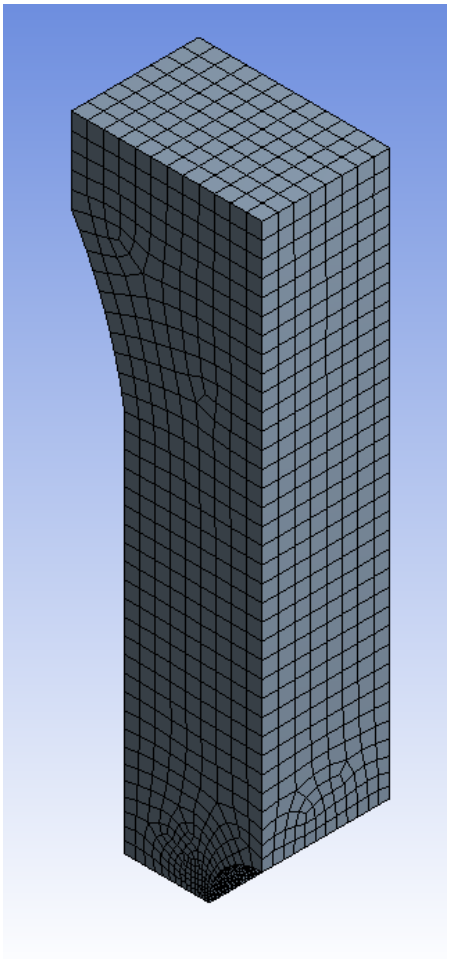

Figure 5.3. ANSYS eighth symmetry mesh of the thick notch specimen.

common methods is to use a fatigue notch factor, K_f, which is divided into the peak stress at the notch root, which is related to and less than the monotonic notch factor, K_t.

It was determined for this geometry that a total knockdown factor of 0.85, or 15% reduction of the calculated value of the PSP and DP at the notch root for life estimation be used. With the knocked down PSP and DP theoretically calculated using the FEA models, theoretical fatigue lives can be pfredicted for the thin and thick specimens, and compared against experimental data.

To aid in the calculation of the DP, a MATLAB script and Microsoft Excel were used to find the plane of maximum shear strain amplitude, and compute the corresponding DP for particular load conditions. After running an FEA model, the time history of the stresses and strains in the xyz coordinate frame, including the shear components, is collected in a Microsoft Excel sheet. The MATLAB script reads the Excel sheet, and computes the DP. The appendix shows a general version of the MATLAB script used for this task.

The MTS axial load frame was used to conduct the experimental fatigue testing for the two notch specimens. Flat wedge grips were used with L brackets attached to properly align the specimens down the centerline of the machine. For the thin notch specimen, shims were used in the grips to close the gap when the pistons reached full capacity. Figures 5.4 and 5.5 show the thin and thick notch specimens, respectively, loaded into the MTS load frame. The tests were run in load control under R = 0 loading conditions, with the number of cycles applied collected until failure.

Once load levels for the two specimens are selected, with the emphasis of creating the same maximum net section stress for both specimens, the FEA models are used to calculate the corresponding PSP and DP for that load level. After using the knockdown factor, the theoretical fatigue lives are calculated, and compared with the experimental fatigue lives of the notch specimens for the given load levels. To get an accurate comparison of the thin notch specimens against the thick notch specimens, the knockdowns will be calculated so that the fatigue models match the thin notch specimens, which should allow a direct comparison for the experimental and theoretical fatigue lives for the thick notch specimens.

It is again noted that the primary objective of this study was to examine the influence of the BR, in order to compare the relative accuracy of the DP versus the PSP. Since there were a

limited number of specimens available, accurate determination of the model constants could not be guaranteed, reducing the confidence level in the actual fatigue life predictions.

Figure 5.4. Thin notch specimen in the MTS load frame.

If the experimental lives did not correlate accurately with the theoretical PSP and DP, an adjustment to the knockdown factor or constants could be made for a better correlation of the data. The PSP, in the case of the notch specimens, was predict a longer fatigue life for the thick notch specimens, since the higher value of the second principal stress (higher BR) would result in a decrease of the equivalent stress amplitude. Conversely, the DP was not expected to predict

much different in lives between the two specimens, since the parameter naturally does not account for the BR in any reasonable capacity.

Figure 5.5. Thick notch specimen in the MTS load frame.

Determining which strain and load levels to use for the final experimental testing is another step that needed to be taken. The next chapter discusses the preliminary analysis using previous experimental data of DA 718

6. PRELIMINARY ANALYSIS

Arbitrary strain and load levels could be chosen in pursuing this study, but previous experimental data would provide a great starting point in determining suitable strain and load levels for the LCF and notch specimens, respectively. This chapter outlines a preliminary material model, constants for the PSP and DP, and the determination of the strain and load levels to be used for the experimental testing.

6.1. Material Model Development

Previous uniaxial LCF data was used to develop a basis for the DA 718 material model. By calculating the material properties from the previous experimental data, initial FEA models of the notch specimens could be analyzed at different load levels to determine which maximum load levels to use for the experimental testing.

Table 6.1 lists previous experimental testing results from LCF DA 718 specimens. All of the data in this table were taken from strain-control tests at R= 0, to mimic the proposed testing conditions of this study.

Table 6.1. DA 718 LCF Experimental Data (R = 0)

ε_{max}	Half-life σ_{max} (ksi)	N_f
0.0070	188.62	26,434
0.0060	175.02	36,914
0.0050	149.80	100,421
0.0065	182.89	28,523
0.0055	163.68	55,888
0.0045	135.42	84,113
0.0047	141.30	141,391

To determine the material constants K' and n' for the Ramberg-Osgood equation, a least-squares fit was used on the plastic strain component from the experimental data using Microsoft Excel. Equations 6.1 and 6.2 below reiterate the necessary formulation to achieve the curve fit.

$$\sigma = K'\left(\varepsilon_{plastic}\right)^{n'} \tag{6.1}$$

$$LCF\ Least\ Squares\ Fit = \sum^{Specimen\ Count}\left[\frac{\left(\sigma_{exp}-\sigma_{theory}\right)}{\sigma_{exp}}\right]^2 \tag{6.2}$$

The material model calculated was from the preliminary analysis used previously for the specimen design. The material properties for the preliminary analysis are listed in table 4.1. The material model provided a method to evaluate the FEA models developed for the two notch specimens when predicting the fatigue life of different load levels.

6.2. Pseudo Stress Parameter and Critical Plane Damage Parameter Development

After the preliminary material model for DA 718 was developed, the PSP and DP constants needed to be fit from a larger experimental data set, with the LCF experimental results from table 6.1 being considered as well. For the fit procedure, uniaxial and torsion data were used, using a least-squares fit method to determine the fatigue constants. Equation 6.3 below shows the least-squares fit procedure for the DP, which was performed in Microsoft Excel.

$$DP\ Least\ Squares\ Fit = \sum^{Specimen\ Count}\left[\frac{DP_{exp}-DP_{theory}}{DP_{exp}}\right]^2 \tag{6.3}$$

DP_{exp} is the experimental DP calculated from the formula, fatigue constants, and applied stress and strain levels, and DP_{theory} is the theoretical DP calculated from the fatigue life relationship using the power law equation. The goal was to minimize the quantity of equation 6.3 while retaining a good curve fit for the theoretical model. The nature of the DP for fit procedures is that it requires both uniaxial and torsion data. The k constant term drops out in torsion loading,

therefore torsion data only cannot be used for an accurate fit. Uniaxial data is then used to help the k constant.

The PSP fatigue constants were fit using a similar procedure as the DP. It was requested that the fit for the PSP model use only the uniaxial, R = 0 LCF data. Even if the other data was not used for the fit, the stress calculations of the thin and thick notch specimens would remain unchanged, with only the predicted fatigue lives varying. Equation 6.4 below shows the least-squares fit for the PSP. Microsoft Excel was used to complete the fit of the constants.

$$PSP\ Least\ Squares\ Fit = \sum^{Specimen\ Count}\left[\frac{PSP_{exp}-PSP_{theory}}{PSP_{exp}}\right]^2 \tag{6.4}$$

PSP_{exp} is the calculated experimental PSP, and PSP_{theory} is the theoretical PSP calculated from the fatigue life equation. The goal was to minimize the value of equation 6.4 for an accurate curve fit.

Table 6.2 shows the uniaxial experimental data with the parameters needed to make calculations for the PSP and the DP. Using the uniaxial data from table 6.2 and unlisted, proprietary torsion data, the least-squares fit procedure for both the PSP and DP was executed using Microsoft Excel. The results of the constants are listed below in table 6.3 for the PSP, and table 6.4 for the DP. Figures 6.1 and 6.2 show the PSP curve fit and DP curve fit, respectively. The two curve fits are based upon stress units of ksi.

Using the calculated fatigue constants, the fatigue life relationships for the PSP and DP are shown in equations 6.5 and 6.6, respectively. The two parameters are used with units of ksi for the stress terms.

$$PSP = \sigma_{eq,a} = 1172.4\left(N_f\right)^{-0.242} \tag{6.5}$$

$$DP = |\tau_{max}|^{.5673}(G\Delta\gamma_{max})^{.4327}\left(1 + .5736\frac{(\sigma|\tau|)_{max}}{\tau_{max}^2}\right) = 392.7\left(N_f\right)^{-.1016} \tag{6.6}$$

Table 6.2. DA 718 Uniaxial Data for Preliminary Fit

R	σ_{max} (ksi)	σ_{min} (ksi)	ε_{max}	ε_{min}	N_f
0	188.62	-22.33	0.0070	0.0000	26,434
0	175.02	-6.07	0.0060	0.0000	36,914
0	149.80	-0.39	0.0050	0.0000	100,421
0	182.89	-13.05	0.0065	0.0000	28,523
0	163.68	-1.90	0.0055	0.0000	55,888
0	135.42	-0.08	0.0045	0.0000	84,113
0	141.30	-0.15	0.0047	0.0000	141,391
-1	135.60	-135.74	0.0045	-0.0045	29,904
-1	105.56	-105.57	0.0035	-0.0035	199,278
-1	120.70	-120.72	0.0040	-0.0040	73,252
-1	97.98	-97.97	0.0033	-0.0033	761,632
-1	113.06	-113.03	0.0038	-0.0038	134,404

Table 6.3. PSP Fatigue Life Constants from Preliminary Fit

Property	Value
Fatigue Coefficient (P)	1,172.4
Fatigue Exponent (z)	-0.242

Table 6.4. DP Fatigue Life Constants for Preliminary Fit

Property	Value
Multiaxial Constant (k)	0.5736
Strain Exponent (w)	0.4327
Fatigue Coefficient (A)	392.70
Fatigue Exponent (b)	-0.1016

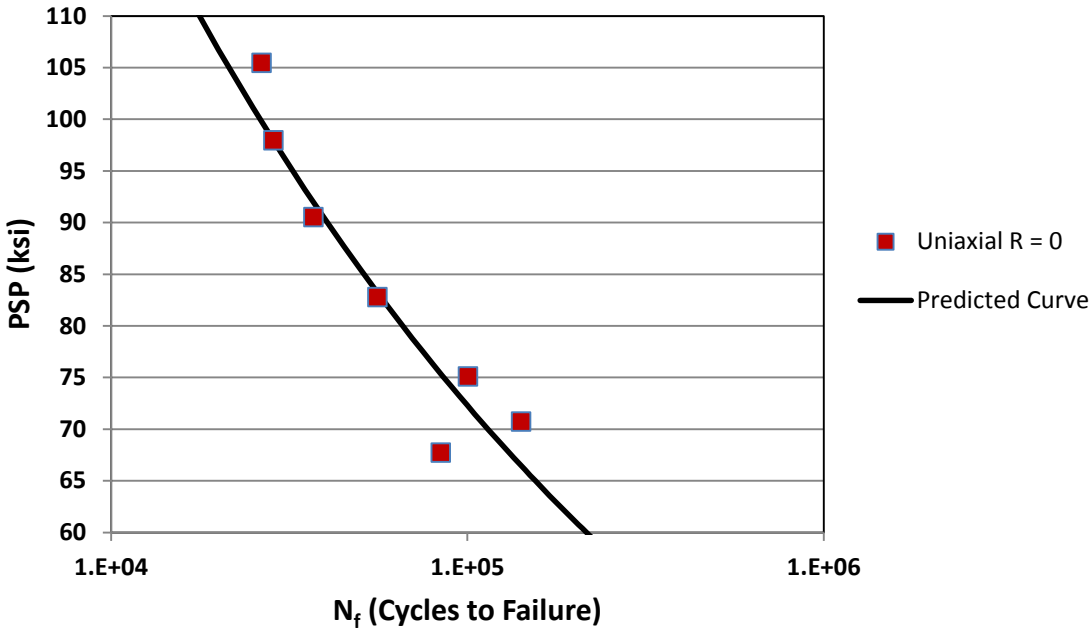

Figure 6.1. PSP curve fit for the preliminary analysis.

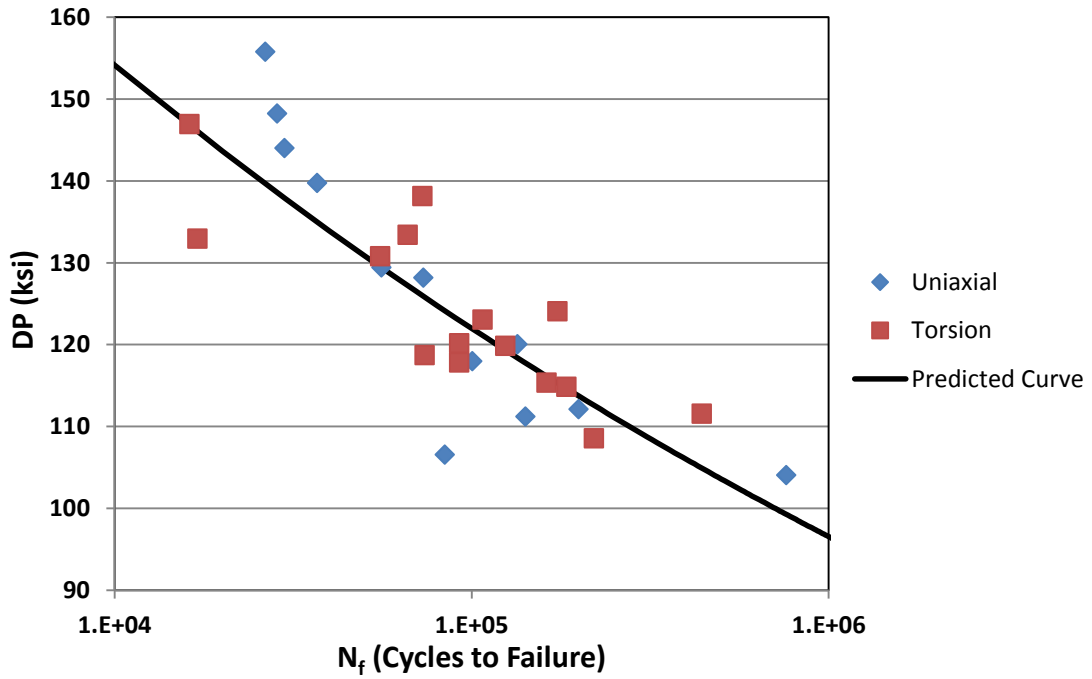

Figure 6.2. DP curve fit for the preliminary analysis.

6.3. Preliminary Finite Element Analysis of Notch Specimens

Using the new multiaxial fatigue models from equations 6.5 and 6.6, along with the preliminary material model, various ANSYS FEA solutions were obtained at different maximum net section stress levels to examine the fatigue life predictions. Table 6.5 below lists the FEA results of the thin notch specimen, and table 6.6 below lists the FEA results of the thick notch specimen. For all fatigue life calculations a knockdown factor of 0.85 was applied to the two fatigue models to account for the stress gradient, and the loading type is R = 0.

Table 6.5. Preliminary FEA Results of Thin Notch Specimen

Max Load (lbf)	$\sigma_{net,max}$ **(ksi)**	**PSP (ksi)**	**PSP N_f**	**DP (ksi)**	**DP N_f**
2500	62.5	60.52	208,407	96.87	911,550
3000	75.0	72.62	98,111	112.34	213,250
3500	87.5	84.73	51,889	127.89	59,824
4000	100.0	96.83	29,884	140.67	23,507
4250	106.3	102.88	23,262	146.47	15,824
4500	112.5	108.94	18,368	151.86	11,100
4750	118.8	114.99	14,691	157.00	8,012
5000	125.0	121.04	11,886	161.84	5,948

Table 6.6. Preliminary FEA Results of Thick Notch Specimen

Max Load (lbf)	$\sigma_{net,max}$ **(ksi)**	**PSP (ksi)**	**PSP N_f**	**DP (ksi)**	**DP N_f**
15000	62.5	56.36	279,642	98.82	749,290
18000	75.0	67.64	131,625	118.59	125,400
21000	87.5	78.91	69,622	132.36	42,717
24000	100.0	90.19	40,093	146.74	15,534
25500	106.3	95.82	31,209	153.08	10,261
27000	112.5	101.46	24,645	159.02	7,067
28500	118.8	107.09	19,711	164.71	5,005
30000	125.0	112.73	15,944	170.09	3,653

Figures 6.3 and 6.4 below display the PSP and DP against their predicted fatigue lives, respectively. The predictions for equation 6.5 show a clear trend of increasing fatigue life in the

thick notch specimen versus the thin notch specimen. On the other hand, the fatigue life predictions for equation 6.6 show a trend of closer fatigue lives, with, in fact, a slight life reduction as the maximum net stresses increase. This trend is most likely due to the onset of plasticity at the higher load levels for the thin notch model compared against the thick notch model.

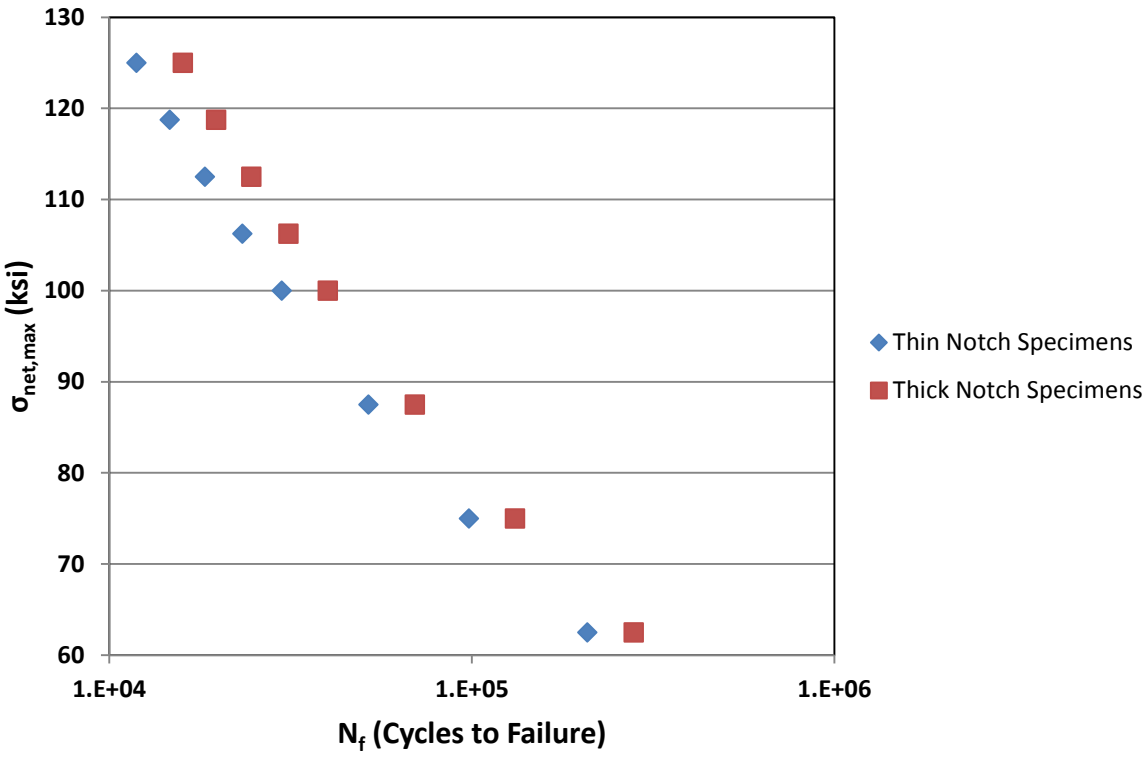

Figure 6.3. PSP versus theoretical fatigue life for the thin and thick notch specimens.

Examining figure 6.4, a strange transition region exists around the 100,000 cycle mark. This is most likely due to the plane stress vs. plane strain effects between the two specimen thicknesses which influences the onset of plasticity. Due to this phenomenon, as well as the ability to perform shorter tests, it was decided that the load level selections would be in the LCF to transition region between 10,000 and 50,000 cycles.

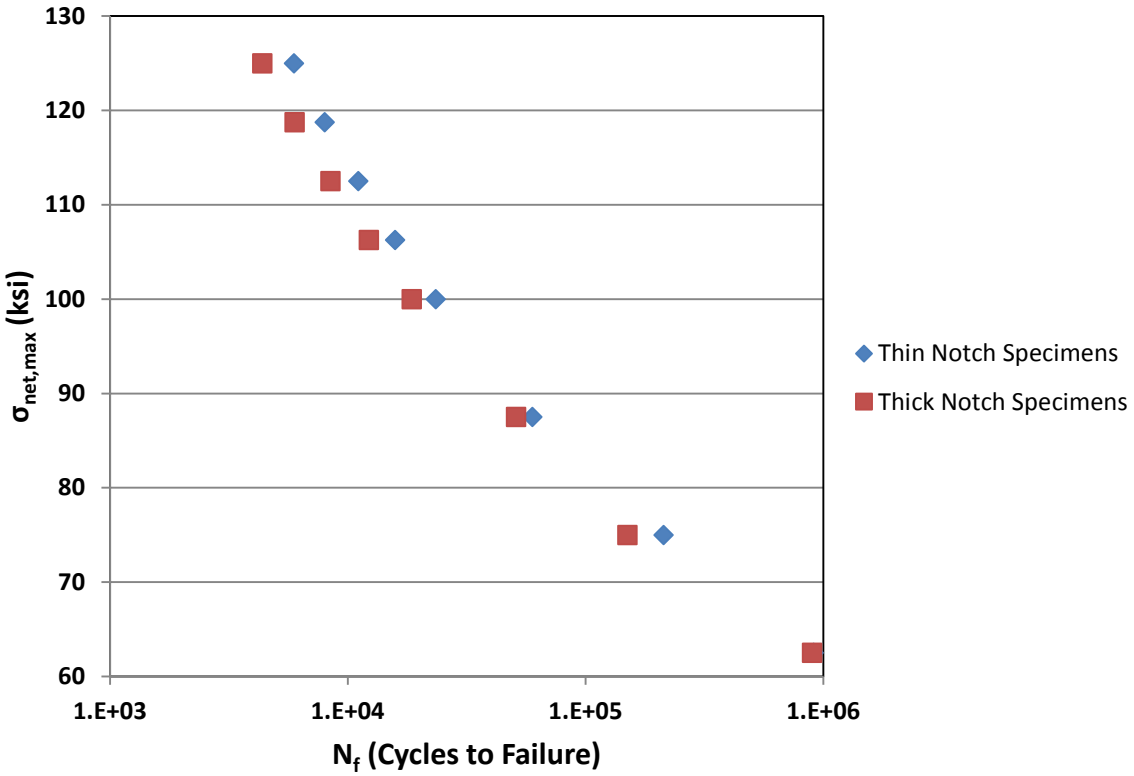

Figure 6.4. DP versus theoretical fatigue life for the thin and thick notch specimens.

6.4. Final Selection of Strain and Load Levels

6.4.1. LCF Specimen Strain Levels

After examination of previous LCF R = 0 experimental data, and with the development of the models, the strain levels chosen are shown below in table 6.7. Particular attention was given to strain levels that would most likely fall between the 10,000 and 50,000 cycle range. It was also appropriate to choose a couple of strain levels that fell before and after that range.

Table 6.7. Experimental R = 0 Strain Level Selections for the LCF Specimens

LCF Specimen	ε_{max} (in/in)
1	0.0045
2	0.0050
3	0.0055
4	0.0060
5	0.0065
6	0.0070
7	0.0075
8	0.0080

6.4.2. Notch Specimen Load Levels

After much consideration, it was decided that only one net stress level for the notch specimens was going to be examined in order to provide a better statistical comparison between the specimens. It was assumed that any behavior and phenomena observed at one net stress level could be extended to other net stress levels. Therefore, the final two load levels that were used for the experimental testing of the notch specimens are shown in table 6.8 below for R = 0 loading.

Table 6.8. Notch Specimen Load Level Selections

Specimen	Net Area (in^2)	Max Load (lbf)	$\sigma_{net,max}$ (ksi)
GENDSU-PO1 (Thin)	0.04	4500	112.5
GENDSU-PO2 (Thick)	0.24	27000	112.5

If the fatigue lives of the thick specimens were typically longer than the thin notch specimens, a life benefit would be present as predicted by the PSP model. On the other hand, if the thick notch specimens had virtually the same or shorter life, no life benefit would be present, showing the DP being more representative of the fatigue lives. If a life benefit is present, an adjustment must be made to the theoretical expression, equation 3.2, to account for the BR. For any life benefit adjustment to the DP, the degree of life benefit must also be considered.

7. RESULTS AND DISCUSSION

For this study, eight LCF specimens and 22 notch specimens were experimentally tested with the MTS axial load frame. The results are examined in this chapter, as well as discussed.

7.1. LCF Specimens

7.1.1. Experimental Results

From the eight LCF specimens, four of the specimens were from the V036 forging, and the other four were from the V038 forging. DA 718 has the potential for the forgings to have different material properties.

During experimental testing, it was observed that the two forgings indeed had slightly different material properties, particularly in the elastic-plastic region. Due to this difference, it was likely that the notch specimens from the two different forgings would also have different fatigue lives for the same net stress levels. Consequently, during experimental testing different strain levels were chosen for the two forgings. Tables 7.1 and 7.2 below show the new strain levels for the V036 and V038 forgings, respectively, for R = 0 strain-control loading.

Table 7.1. V036 Experimental Strain Levels

Specimen ID	$\boldsymbol{\varepsilon_{max}}$ **(in/in)**
V036-A-T1	0.0055
V036-B-T1	0.0065
V036-D-T1	0.0070
V036-C-T1	0.0080

Table 7.2. V038 Experimental Strain Levels

Specimen ID	$\boldsymbol{\varepsilon_{max}}$ **(in/in)**
V038-C-T1	0.0050
V038-B-T1	0.0065
V038-D-T1	0.0065
V038-A-T1	0.0075

During experimental testing, two specimens experienced difficulties while in strain-control. Specimen V036-D-T1 became unstable during operation and was overstrained by more than ten percent. Since the strain levels chosen were already in the elastic-plastic region of the material, the over-strain resulted in a mean-stress reduction when the strains were returned to the desired levels, yielding a longer than expected fatigue life. The other specimen that experienced difficulties was specimen V038-D-T1, which experienced an unstable elevation in load level and failed in a fast, monotonic behavior. This was most likely due to a slip of the extensometer during operation. Due to these difficulties, the two specimens were not included with the final results for the material models, and fatigue model fit process.

The final LCF experimental results are listed in table 7.3 for the V036 forging, and table 7.4 for the V038 forging below. Listed are the fatigue lives, the half- life (HL) maximum load levels, and a description of the failure of the specimen.

Table 7.3. V036 Final Experimental Results

Specimen ID	**N_f**	**HL Max Load (lbf)**	**Description**
V036-A-T1	68,457	13,695	Failure at gage section
V036-B-T1	36,007	15,251	Failure at gage section
V036-D-T1	45,228	---	Overstrain error
V036-C-T1	23,792	15,239	Failure at gage section

Table 7.4. V038 Final Experimental Results

Specimen ID	**N_f**	**HL Max Load (lbf)**	**Description**
V038-C-T1	80,341	13,180	Failure at gage section
V038-B-T1	28,955	15,386	Failure at gage section
V038-D-T1	---	---	Monotonic error
V038-A-T1	26,676	15,949	Failure at gage section

Figure 7.1 below shows the results of the LCF specimens, with the two invalid specimens discarded. As suspected, the two forgings had slightly different material properties and fatigue lives.

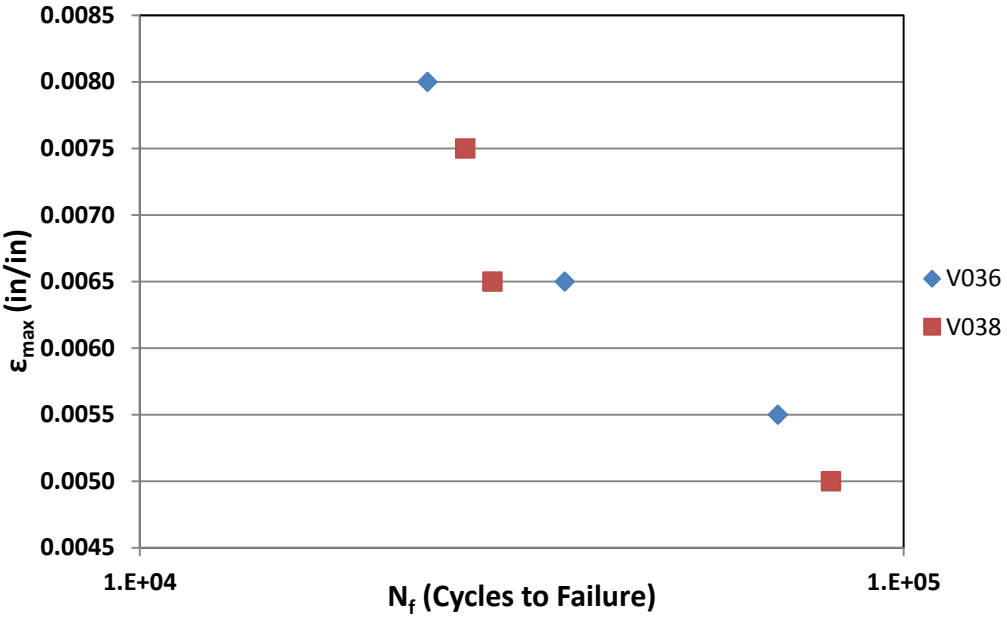

Figure 7.1. Experimental results for the LCF specimens.

7.1.2. Material Models

Due to the material property differences between the two forgings, it was determined that two different material models would be needed. From the experimental results, the V036 forging indicated a more ductile material behavior in the elastic-plastic region and slightly lower yield strength as well. The two models were fit using a least-squares fit. The plastic true strains and corresponding stresses at the maximum strain levels were computed at the half-life of the LCF specimens from the experimentally collected data.

To determine the cyclic yield strength, the common method is to use the definition of the 0.2% offset yield stress from the hysteresis loop at the half-life of the specimen. Plasticity was present in the specimens, but the plastic strain levels were very small, with the highest plastic strain for all specimens reaching 0.001 or 0.1% strain. This combined with the MKH model and the fit of the Ramberg-Osgood coefficients, the cyclic yield strength needed to be much closer to the curve instead of using an offset method. It was decided to use the first cycle from the experimental data, and use an approximation of the proportional limit stress. In practice the offset method is more acceptable; due to the small amount of plasticity, an approximate material model using an approximate proportional limit stress was deemed acceptable for this study.

The V036 forging material model was analyzed and fit using Microsoft Excel, with the plastic true strains and stresses of the three valid LCF specimens. During experimental testing, the V036-C-T1 LCF specimen showed strong cyclic softening, as the load on the specimen dropped from 16,000 lbs at the beginning of the test to 15,239 lbs at half-life. The other specimens, however, did not experience such a significant load relaxation during fatigue testing. Despite this anomaly, the material model for the V036 forging used all three specimens. Table 7.5 lists the material properties for the V036 forging, with figure 7.2 showing the true stress versus plastic strain curve.

Table 7.5. V036 Material Properties

Property	Value
Elastic Modulus (E)	30,800 ksi
Poisson's Ratio (υ)	0.311
Cyclic Strain Hardening Coefficient (K')	247.5 ksi
Cyclic Strain Hardening Exponent (n')	0.0493
Cyclic Yield Strength (σ_y')	158.33 ksi
Ultimate Strength (σ_{ut})	260.12 ksi

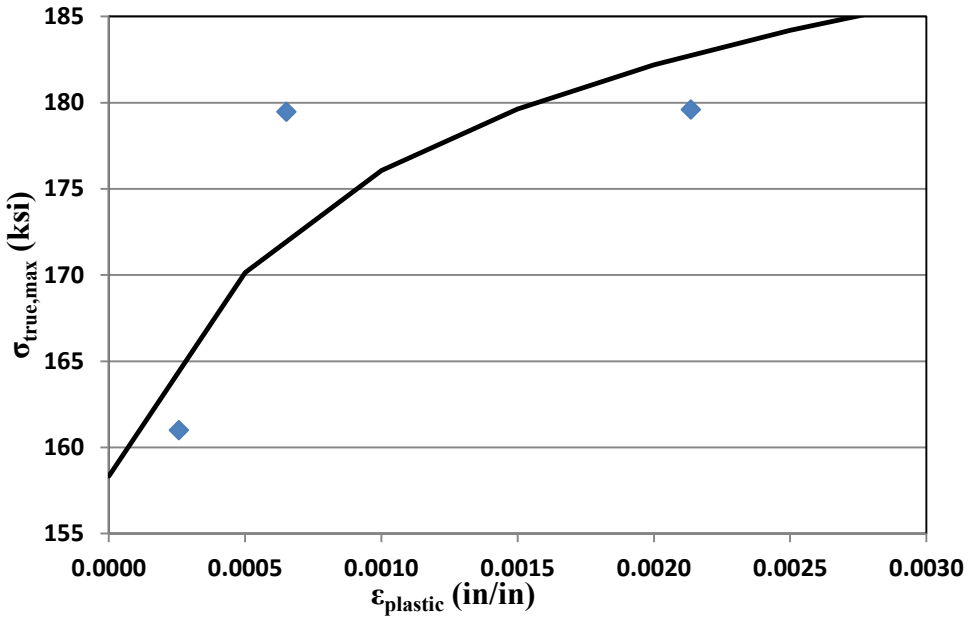

Figure 7.2. V036 stress-plastic strain curve.

The V038 forging material model was constructed using the same techniques as the V036 material model. However, of the three valid V038 LCF specimens, only two were in the elastic-plastic region of the material. The V038-C-T1 LCF specimen was completely elastic, and could not be used to fit the Ramberg-Osgood coefficients. This provided only two points to develop the Ramberg-Osgood coefficients for plasticity, which doesn't provide the most accurate material model for plasticity. Due to the nature of this study, however, two points were deemed adequate to develop the V038 material model. Table 7.6 shows the material model for the V038 forging, with figure 7.3 plotting the true stress versus plastic strain curve.

Table 7.6. V038 Material Properties

Property	Value
Elastic Modulus (E)	30,300 ksi
Poisson's Ratio (υ)	0.311
Cyclic Strain Hardening Coefficient (K')	244.9 ksi
Cyclic Strain Hardening Exponent (n')	0.0398
Cyclic Yield Strength (σ_y')	160 ksi
Ultimate Strength (σ_{ut})	260.12 ksi

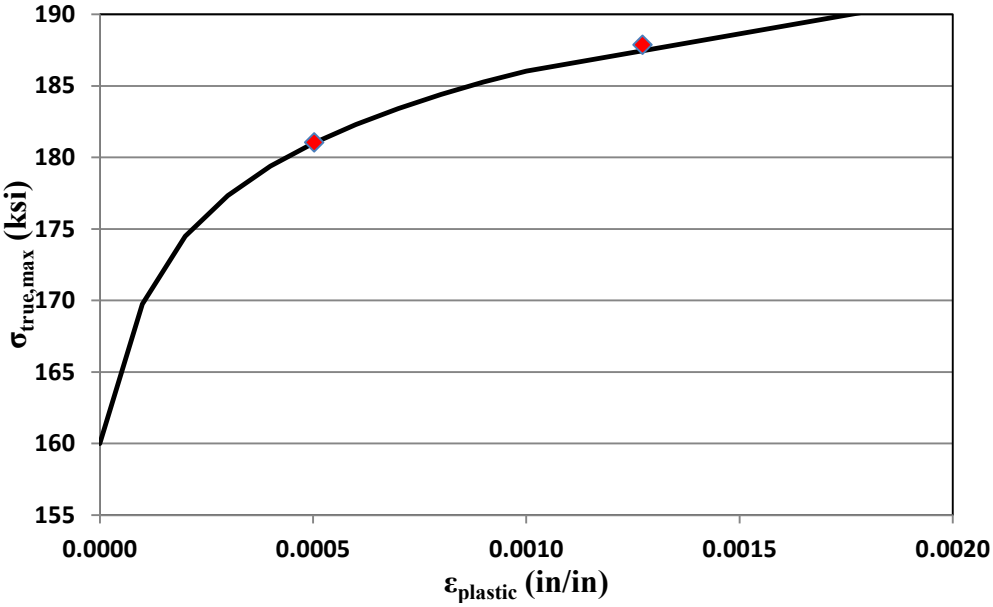

Figure 7.3. V038 stress-plastic strain curve.

7.1.3. Fatigue Models

Since two different material models were used for two different forgings, it was determined that two sets of fatigue models would be used, one for the V036 forging and one for the V038 forging. Microsoft Excel was used with a least-squares fit to generate the curves for the PSP and DP power law equations. The DP constants *k* and *w* were held constant using the preliminary analysis values with the assumption that the damage mechanisms and behavior

between different pedigrees of DA 718 were similar and equal for this study. This reduced the constants to two instead of four in the DP equation fit.

The V036 fatigue models were fit using the three LCF specimens with a least-squares fit. This resulted in the PSP constants in equation 3.3 and the DP constants in equation 3.4 shown in tables 7.7 and 7.8, respectively. Following are figures 7.4 and 7.5, which show the PSP and DP curve fits, respectively, for the V036 fatigue models with units of ksi.

Table 7.7. V036 PSP Constants

Property	Value
Fatigue Coefficient (P)	3,908.76
Fatigue Exponent (z)	-0.3463

Table 7.8. V036 DP Constants

Property	Value
Multiaxial Constant (k)	0.5736
Strain Exponent (w)	0.4327
Fatigue Coefficient (A)	1,186.20
Fatigue Exponent (b)	-0.2012

Observing figures 7.4 and 7.5 the V036 fatigue models show great correlation, especially the DP fatigue model. These models were adequate to use for fatigue life calculations using FEA modeling and classical calculations.

The V038 fatigue models were fit using the LCF specimens with a least-squares fit. Tables 7.9 and 7.10 show the PSP and DP curve fits, respectively, followed by figures 7.6 and 7.7, which show the PSP and DP curve fits, respectively. The constants are fit with units of ksi. Observing figures 7.6 and 7.7, the V038 fatigue models show fair correlation, and were deemed adequate for this study.

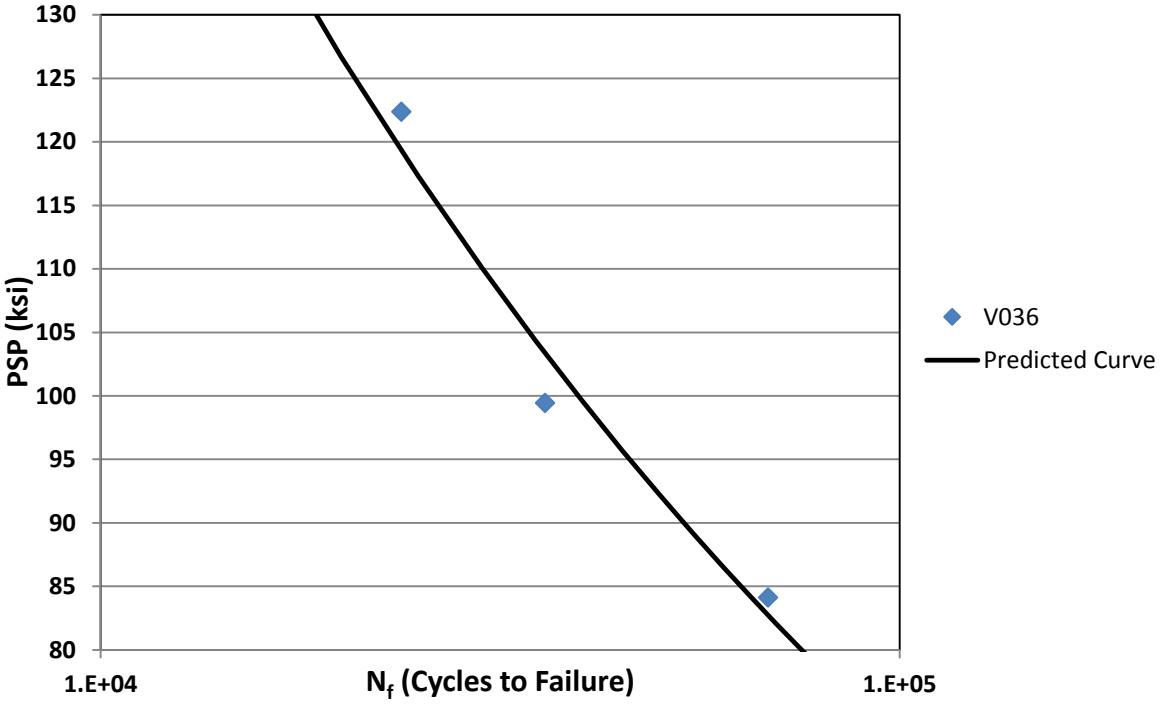

Figure 7.4. V036 PSP model curve fit.

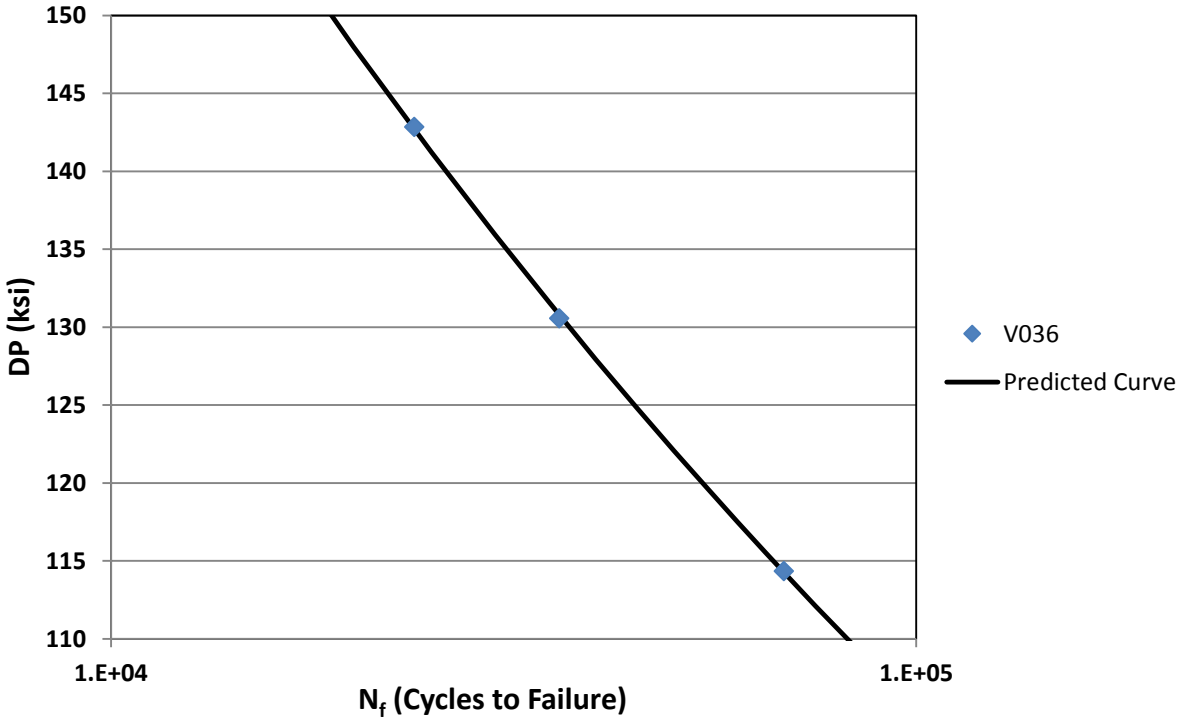

Figure 7.5. V036 DP model curve fit.

Table 7.9. V038 PSP Constants

Property	Value
Fatigue Coefficient (P)	3,908.76
Fatigue Exponent (z)	-0.3509

Table 7.10. V038 DP Constants

Property	Value
Multiaxial Constant (k)	0.5736
Strain Exponent (w)	0.4327
Fatigue Coefficient (A)	1186.20
Fatigue Exponent (b)	-0.2079

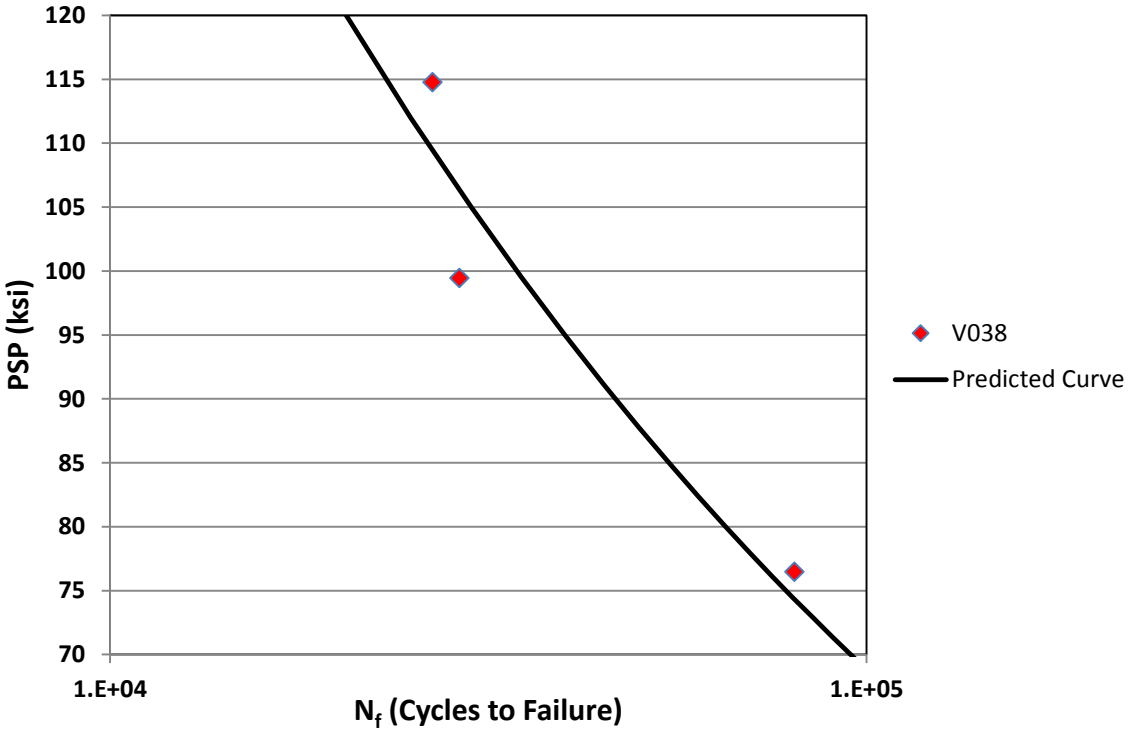

Figure 7.6. V038 PSP model curve fit.

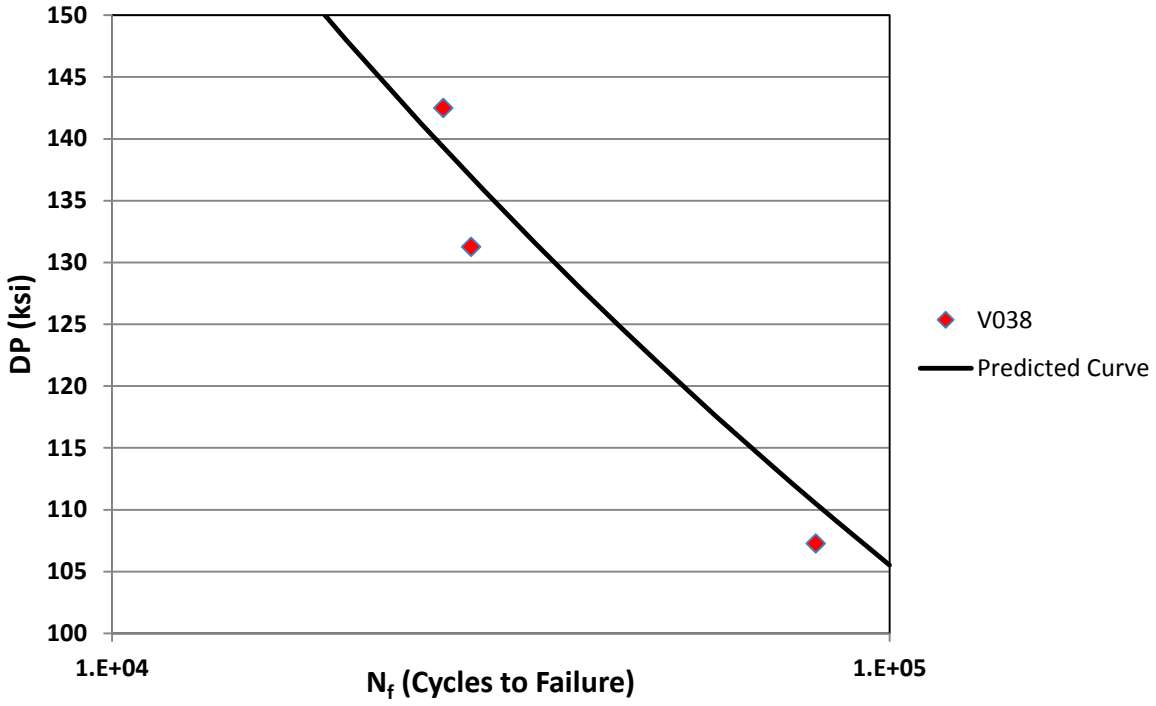

Figure 7.7. V038 DP model curve fit.

7.2. Notch Specimens

7.2.1. Experimental Results

22 notch specimens were experimentally tested in the MTS axial load frame, which were divided into 11 thin notch specimens and 11 thick notch specimens. For the thin notch specimens, six were from the V038 forging, while the other five were from the V036 forging. For the thick notch specimens, six were from the V038 forging, while the other five were from the V036 forging.

All of the specimens were tested at R = 0 loading with a maximum net stress of 112.5 ksi. This translated to a maximum load level of 4,500 lbs for the thin notch specimens, and 27,000 lbs for the thick notch specimens. No specimens experienced any noticeable problems during testing, such as overstrains or monotonic error, with all specimens failing in the notch section.

Examining the specimens, no major anomalies were spotted with respect to crack initiation locations or propagation. Due to the material property differences between the V036 and V038 forgings, it was expected that the V036 forging notch specimens would produce fatigue lives longer than the V038 forging notch specimens due to their higher fatigue resistance shown in the LCF specimens.

Tables 7.11 and 7.12 below show the experimental fatigue lives of the thin and thick notch specimens, respectively, from the V036 forging. For the thin notch specimens, the average fatigue life was 29,816 cycles, with a standard deviation of 2,033 cycles. For the thick notch specimens, the average fatigue life was 37,203 cycles, with a significantly higher standard deviation of 4,060 cycles, a much larger scatter compared to the thin notch specimen counterparts.

Table 7.11. V036 Thin Notch Specimen Fatigue Lives

Specimen ID	**N_f**
V036-C-BH1	29,347
V036-C-BH2	32,144
V036-C-BH3	28,059
V036-D-BH1	31,740
V036-D-BH2	27,790

Table 7.12. V036 Thick Notch Specimen Fatigue Lives

Specimen ID	**N_f**
V036-A-BH1	39,429
V036-A-BH2	34,709
V036-A-BH3	35,508
V036-B-BH1	43,182
V036-B-BH2	33,185

The fatigue lives of the V038 thin and thick specimens are shown below in tables 7.13 and 7.14, respectively. For the thin notch specimens, the average fatigue life was 26,945 cycles,

with a standard deviation of 2,924 cycles. For the thick notch specimens, the average fatigue life was 28,754 cycles, with a standard deviation of 1,852 cycles.

Table 7.13. V038 Thin Notch Specimen Fatigue Lives

Specimen ID	N_f
V038-C-BH1	30,138
V038-C-BH2	29,688
V038-C-BH3	25,827
V038-D-BH1	28,155
V038-D-BH2	22,491
V038-D-BH3	25,372

Table 7.14. V038 Thick Notch Specimen Fatigue Lives

Specimen ID	N_f
V038-A-BH1	31,923
V038-A-BH2	26,868
V038-A-BH3	29,838
V038-B-BH1	28,545
V038-B-BH2	27,630
V038-B-BH3	27,718

7.2.2. Theoretical Results

To complete the theoretical calculations for the fatigue lives of the thin and thick notch specimens, the ANSYS FEA models developed previously were used with the new material models. Due to the V036 and V038 forgings having different material properties, derived from the LCF specimens, four different FEA models were needed, with two of the models for the thin notch specimen with the two material models, and two of the models for the thick notch specimen with the two material models. Using ANSYS to complete the analysis set, the final theoretical results are shown in table 7.15 below. These results do not include the knockdown factor needed to account for the stress gradient effect in the notch specimens. The critical plane

MATLAB script that was developed was used to calculate the DP, which aided the speed of the process. The PSP theoretical calculations were simply drawn from the ANSYS equivalent stress values.

Table 7.15. Final Theoretical Results for Notch Specimens

Theoretical Model	PSP (ksi)	DP (ksi)
V036 Thin Notch Specimen	128.2	171.7
V036 Thick Notch Specimen	119.4	177.2
V038 Thin Notch Specimen	128.2	175.2
V038 Thick Notch Specimen	119.4	180.8

7.2.3. Comparison of Experimental and Theoretical Results

The theoretical PSP and DP values in table 7.15 were calculated from the stress and strain states at the notch roots of the specimens. To account for the stress gradient effect of the notch specimens, a knockdown factor, similar to the fatigue notch factor, was used to reduce the PSP and DP to more accurate values.

When examining the PSP and DP, if a knockdown factor of 0.85 was used, the theoretical fatigue lives did not match well with the experimental fatigue lives. To better account for this mismatch, the knockdown factor was modified so that the thin notch specimen average experimental fatigue lives matched the theoretical fatigue lives, which provided a baseline to compare the theoretical and average experimental fatigue lives of the thick notch specimens relative to the thin notch specimens.

Using Microsoft Excel, new knockdown factors were calculated to match the thin notch specimen experimental and theoretical fatigue lives together for both forgings. This resulted in table 7.16 below, which shows the final comparison between the experimental and theoretical fatigue lives. Knockdown factors needed to be calculated for both the PSP and the DP for each forging.

Table 7.16. Experimental vs. Theoretical Fatigue Lives

Specimen	Avg. N_f	PSP KD	PSP N_f	PSP %	DP KD	DP N_f	DP %
V036 Thin	29,816	0.861	29,816	0.00%	0.820	29,816	0.00
V036 Thick	37,203	0.861	36,616	-1.58%	0.820	21,825	-41.34%
V038 Thin	26,945	0.851	26,945	0.00%	0.812	26,945	0.00
V038 Thick	28,754	0.851	33,001	14.77%	0.812	23,190	-19.35%

7.3. Discussion

7.3.1. Examination of Results

Examining the results, there was a clear trend that the thick notch specimens had a fatigue life benefit over the thin notch specimens, due to the BR being higher in the thick notch specimens than the thin notch specimens. For both of the forgings, the PSP predicted a fatigue life benefit for the thick notch specimens in comparison to the thin notch specimens, as expected. Conversely, the DP predicted a slight fatigue life reduction for the thick notch specimens versus the thin notch specimens. The overall experimental results agreed more with the PSP as a theoretical model than the DP, but the life benefits it produced for the specimens, especially the V038 forgings, might be too excessive.

In the V036 forging specimens, the thick notch specimen average fatigue life was close to its corresponding PSP prediction, and in fact exceeded the predicted, theoretical fatigue life of the thick notch specimen. However, the scatter of the fatigue lives of the thick notch specimens, as shown in the standard deviation, indicated uncertainty in the value of the average fatigue life of the thick notch specimens. It was possible that the thick notch specimens encountered some statistical variations, especially since the lowest fatigue life of the thick notch specimens was 33,185 cycles. Though this indicates a life benefit, it is considerably less than the predicted PSP fatigue life. Clearly the DP fatigue life prediction of the thick notch specimens was not correct,

as it predicted a slight reduction in comparison to the thin notch specimens of the V036 forging, which showed much better consistency and less scatter.

Examining the specimens from the V038 forging, the thick notch specimens average fatigue life indicated a life benefit, with a relatively tight scatter, versus the thin notch specimens. With a life benefit present, the PSP overpredicted the fatigue life considerably, while the DP predicted a life reduction in the thick notch specimens compared against the thin notch specimens. Overall, the V038 specimens had good distribution, with the thin notch specimens having a little more scatter than the thick notch specimens.

Based upon the experimental data, each fatigue model did not necessarily fit the trend of the data for the overall data set.

The PSP did give a life benefit to the thick notch specimens, but the V038 thick notch specimen average life benefit was less than half of what the PSP predicted. For the V036 specimens, the PSP slightly underpredicted the fatigue life of the thick notch specimens, but with the higher amount of scatter, uncertainty existed in the average fatigue life value of thick notch specimens.

For the specimens from both forgings, the DP predicted a fatigue life reduction in the thick notch specimens with respect to the thin notch specimens. Even in the V038 notch specimens, a life benefit was consistently present in the thick notch specimens. Despite the high amount of scatter in the V036 thick notch specimens, the lowest fatigue life of those specimens was 33,185 cycles, which is higher than the average of 29,816 cycles for the thin notch specimens. Therefore, the DP was not accurate with its fatigue life reduction of the thick notch specimens.

7.3.2. Fatigue Models Evaluation

The comparison of the experimental and theoretical results indicates that the equivalent stress parameter, the PSP, might need a fatigue life reduction term since it might naturally overpredict the theoretical life in the case of higher BRs. This is also compounded by the method used to compute the PSP, which uses a purely elastic model, and not an elastic-plastic model, which could change the calculation of the fatigue life.

Conversely, the DP needs a term to add a fatigue life benefit, since the BR difference between the specimens has been shown to influence the total fatigue life. This was a likely outcome, since the DP doesn't account for the secondary stress or strain component, or the second principal stress or strain in the case of proportional loading.

The results of this study were consistent with the findings of past studies, especially the study performed by Lefebvre [37]. This study mutually concludes that equivalent stress parameters, such as the PSP, need a fatigue life reduction factor in the cases of high BRs when the third principal stress is close to zero, while critical plane parameters, such as the current DP, need to account for the secondary stress and/or strain effects, which can add a fatigue life benefit.

7.3.3. Secondary Considerations

Since the notch specimens have a stress gradient effect during loading, the crack propagation life of the specimens might be different between the two notch specimens in the direction of the thickness. However, since the PSP and DP were fit using failure lives of the LCF specimens, the crack propagation life was not considered in the analysis and fatigue models were deemed adequate for life prediction.

Typically, critical plane parameters are used to predict the crack initiation life, but since the constants for both fatigue models were fit using failure lives, this was not deemed an issue

for this study. A crack propagation life analysis was performed for both notch specimen geometries, and determined that the thick notch specimen did have a longer crack propagation life than the thick notch specimen. If the crack initiation lives were used to the fit the DP, the constants would change to account for the new definition of failure.

Another possible fatigue life influence was a misalignment of the MTS axial load frame and the L-brackets used to center the notch specimens on the flat grips. To help combat this possible problem, the load frame was checked for accurate alignment, as discussed earlier in this study, and the notch specimens were checked once loaded into the frame for L-bracket alignment verification. No major misalignment was seen in the machine and L-brackets, and the experimental results showed good data correlation and relatively tight scatter for the nature of this study. Misalignment was ruled to have little to no influence on the fatigue lives of the specimens.

7.3.4. Discussion Summary

The experimental results of the notch specimens show that a fatigue life benefit does exist in the thick notch specimens for both forgings. The PSP predicted fatigue life benefits for both sets of thick notch specimens. However, the fatigue life benefits present in the experimental data, particularly in the V038 thick notch specimens, indicated that the life benefits might not be as much as the PSP predictions. The DP predicted fatigue life reductions in the thick notch specimens for both forgings, but the experimental data clearly indicated that a fatigue life benefit was present in the thick notch specimens, meaning the DP must be modified to include the effects of the BR. The modification of the DP is discussed in the next chapter.

8. PROPOSED CRITICAL PLANE MODEL

The results of this study indicated that a fatigue life benefit term was needed in the current DP. This chapter discusses the development of a new, proposed fatigue model to take in account the effects of the secondary stress on multiaxial fatigue life.

8.1. Development of Critical Plane Model

8.1.1. Effect of Secondary Stress on Equivalent Stress

The secondary stress in multiaxial fatigue can greatly influence the calculation of fatigue life, particularly in equivalent stress models that use the von Mises definition. In this study, the BR was used as a benchmark to compare the thin and thick notch specimens, since the third principal stress was very close to zero. However, when looking at the principal stresses, the second principal stress must fall between the first and third principal stresses, which means that though the BR might be 0.5, for instance, it doesn't mean that a life benefit is occurring.

Figure 8.1 below shows the von Mises stress as a function of the BR. For figure 8.1, the first principal stress and third principal stress are 100 and -100, respectively, with units ignored for concept. Notice that the smallest von Mises stress, corresponding to the greatest life benefit, is given when the second principal stress is zero, for this example. In this case, the maximum shear stresses in the 1-2 and 2-3 planes are equal. As the second principal stress departs from zero, the maximum shear stress in the 1-2 plane will increase if the BR decreases, or the maximum shear stress in the 2-3 plane will increase if the BR increases. Regardless, the von Mises definition, which the PSP uses, the greatest life benefit occurs when the 1-2 and 2-3 plane maximum shear stresses are equal.

In the case of this study, the von Mises definition of the PSP predicted a life benefit naturally for the thick notch specimen due to the maximum shear stresses in the 1-2 and 2-3

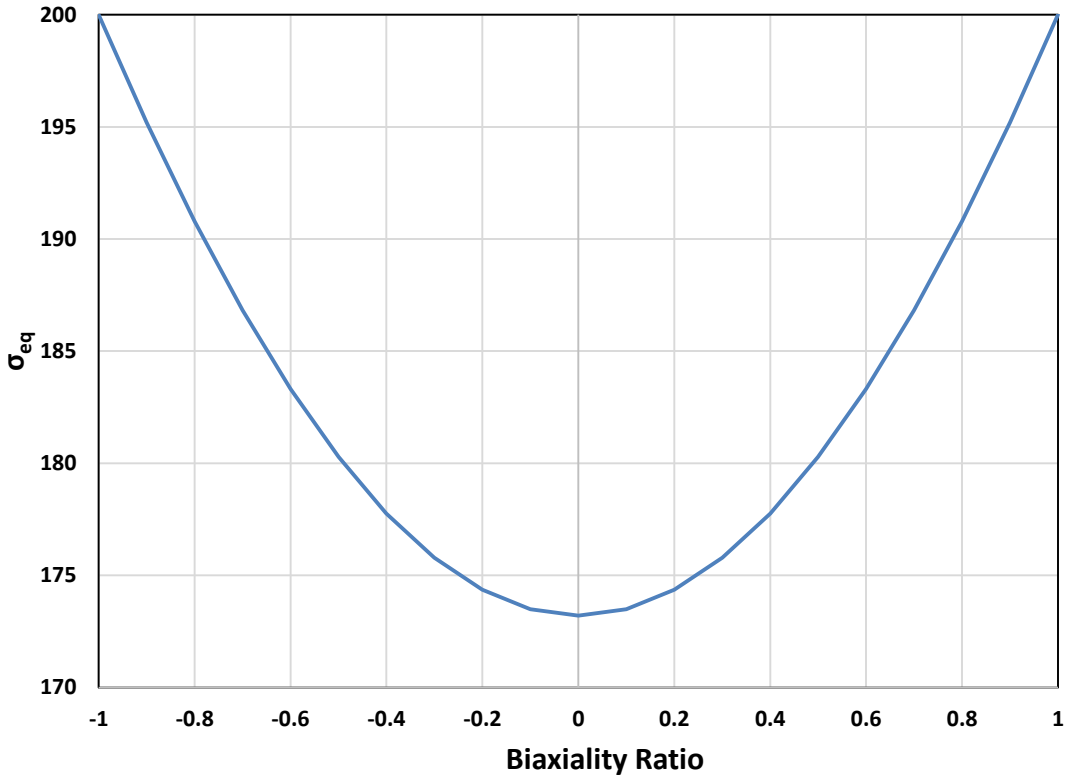

Figure 8.1. Example comparison of the von Mises stress versus the BR.

planes moving toward equality. Though the von Mises definition of yielding for metals has been shown to correlate well in monotonic testing, it does not physically represent fatigue crack nucleation or propagation and is a scalar value. Tension and compression can have different effects on crack initiation, and can either aid or inhibit crack opening. In the case of the equivalent stress definition for the example above, the second principal stress can be compressive or tensile, and still give the same equivalent stress value. In the case of this study, the third principal stress was almost zero, meaning that the greatest life benefit for the PSP was at a BR of 0.5.

8.1.2. Physical Definition of Proposed Critical Plane Model

The proposed critical plane parameter attempts to describe physical characteristics in its formulation. In ductile metals, it is known that generally cracks initiate on or near planes of

maximum shear stress range or maximum shear strain range, which contributes to the distortion of the material, or deviatoric term of the stress and strain tensors. The current DP used for this study uses a physical definition similar to the Fatemi-Socie [23] critical plane model, shown previously in figure 2.1. Cracks initiate on planes of maximum shear strain amplitude, while stresses normal to the critical plane promote crack opening. The current DP does not account for secondary stress or strain, which has been shown in the results of this study to have an effect on the fatigue life of metallic materials. The current DP needed to be modified to account for this secondary effect.

This study proposes an addition to the physical definition of the current DP, which was based upon the Fatemi-Socie [23] model. In the proposed physical definition, including the maximum shear stress/strain range creating cracks and normal stresses opening the cracks, the secondary stress exists and its direction is normal to the plane created by the vector of the shear strain range and normal stress opening the crack. The material that contains the crack is treated as two membranes that are fastened by the uncracked portion of the material.

As the secondary stress pulls in tension, the material response will be to close the crack together due to the material experiencing a compressive strain in the direction normal to the critical plane. When the secondary stress is compressive, the material will respond by opening the crack due to a positive strain in the direction normal to the critical plane. Figures 8.2 and 8.3 below illustrate this physical definition of the proposed DP when the secondary stress is tensile and compressive, respectively.

Physically, the tensile secondary stress will try to stretch close the crack, which can aid in keeping the crack closed, while the compressive secondary stress will attempt to open, or "buckle" the two membranes above and below the crack, creating more damage.

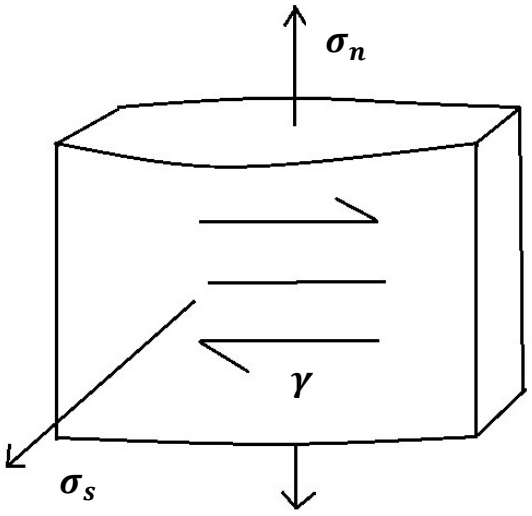

Figure 8.2. Physical illustration of crack closing from tensile secondary stress.

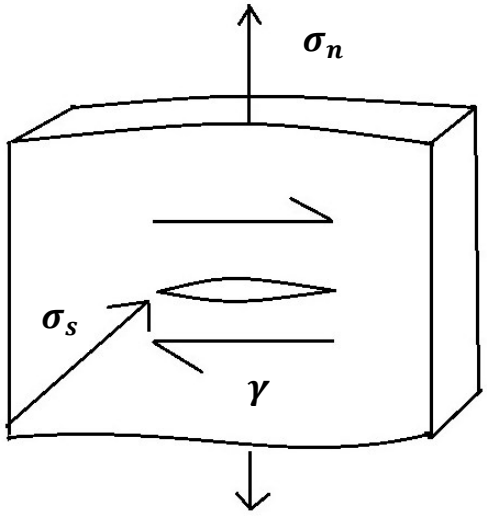

Figure 8.3. Physical illustration of crack opening from compressive secondary stress.

8.1.3. Application to Proposed Critical Plane Model

The current damage parameter, equation 3.2, uses the physical damage mechanisms without accounting for the secondary stress or strain component. The proposed critical plane model, DP_{prop}, modifies the maximum shear stress term in equation 3.2 with a new constant that allows scalability to different materials using this new model. When the DP was analyzed

between the thick and thin specimens, the first term containing the maximum shear stress on the critical plane is what drove the term to higher values in the thick notch specimens, while the other two terms were relatively equal between each other. Therefore, a modification to the first term was used to include the influence of the secondary stress.

$$DP_{prop} = \left(|\tau_{max}| - k_1\sigma_{s,mean}\right)^{1-w}(G\Delta\gamma_{max})^{w}\left(1 + k_2\frac{(\sigma|\tau|)_{max}}{\tau_{max}^2}\right) = A\left(N_f\right)^{b} \qquad (8.1)$$

In the new model above, k_1 is a new constant that scales the mean stress in the secondary direction, $\sigma_{s,mean}$, against the maximum shear stress over the loading cycle. The constant k_2 is just a replacement for the constant k in equation 3.2.

The cyclic mean stress was chosen over the maximum stresses since the damaging effect could either benefit or reduce the fatigue life. When the secondary mean stress is tensile, the term will reduce the maximum shear stress term, therefore extending the fatigue life of the specimen. If the secondary mean stress is compressive, the term will actually become negative, thereby increasing the maximum shear stress term, reducing the total fatigue life. If maximum terms were used, the secondary stress might possibly spend much of the loading cycle in compression, but use a life benefit since the maximum secondary stress might be positive, or vice versa for tension. It is unclear if another definition, such as the maximum stress or strain, should be used.

To fit equation 8.1 to experimental data, torsion, uniaxial, and biaxial data are needed, since the constant k_1 requires a secondary stress be available for the fit procedure. Uniaxial and torsion data do not have secondary stress terms in the way equation 8.1 is defined, therefore biaxial data is needed to account for the secondary stress term.

8.2. Validation of Proposed Model

An initial analysis was done using the existing experimental results from this study. With the proposed critical plane model, the thin and thick notch specimen fatigue lives needed to be recalculated for each of the forgings.

8.2.1. Initial Analysis

To test the feasibility of the proposed fatigue model, the thin notch specimen average fatigue lives were used as a basis to test against the thick notch specimens. Originally, knockdown factor of 0.85, or 85%, was used for the fatigue model adjustment due to the stress gradient effect. To fit the new constant, k_1, the computed DP from the original single power law constants A and b would be used in conjunction with the original knockdown factor using the experimental average fatigue life of the thin notch specimens for each forging. Due to the nature of equation 8.1, a refit of the constants k_2 and w was not needed, using the old constants from equation 6.6 in the original theoretical analysis for each forging, since the k_1 naturally drops out from equation 8.1 when used for uniaxial and torsion modeling.

Using the proposed DP, equation 8.1, the new constant k_1 was fit using the experimental average fatigue life of the thin notch specimens with the two different forgings. After this step, the theoretical fatigue lives calculated for the thick notch specimens was compared against the experimental average fatigue life for each forging, checking the accuracy of the proposed model. This produced the results, shown in table 8.1 below, with all other constants remaining equal, using the original knockdown factor of 0.85.

Table 8.1 shows promising results for the proposed critical plane model. For the V036 thick notch specimen, the proposed model predicts the experimental average fatigue life within 6.89%, while for the V038 thick notch specimen, the proposed model predicts the experimental

average fatigue life within the scope of 3.84%. This correlation was a great improvement over the current DP, which significantly underpredicted the total fatigue lives of the thick notch specimens

Table 8.1. Proposed Critical Plane Model Analysis with Experimental Results

Notch Specimen	Avg. N_f	k_1	DP_{prop} N_f	DP_{prop} %
V036 Thin	29,816	0.8200	29,880	0.22%
V036 Thick	37,203	0.8200	39,957	6.89%
V038 Thin	26,945	0.5544	26,891	-0.20%
V038 Thick	28,754	0.5544	29,901	3.84%

While the PSP predicted a fatigue life close to the experimental average value for the V036 forging, the PSP grossly overpredicted the fatigue life of the V038 forging by over 14%. This means the proposed critical plane model in equation 8.1 shows potential for multiaxial fatigue life prediction, while accounting for the secondary stresses during the loading cycle. The average experimental and theoretical fatigue lives don't completely match up due to significant figure differences, but matched adequately for comparison.

The initial analysis also indicates that the new constant k_1 is possibly a function of the material, and can account for how different materials react under multiaxial fatigue to the secondary stress effect. For the proposed fatigue model, all of the constants would be a function of material properties of each of the forgings, but due to the low amount of specimens available for accurate material models, it was assumed that the k_2 and w constants were virtually the same, and remained unchanged between the two forgings.

8.2.2. Discussion of Proposed Critical Plane Model

The proposed critical plane model in equation 8.1 shows promising results when comparing the experimental results of this study against the predicted fatigue lives from the material models of the forgings. To fit the proposed model, three types of specimens are needed,

which are torsion, uniaxial, and biaxial specimens. If biaxial specimens are not available and not needed, the constant k_1 can be dropped by setting the value equal to zero, which will reduce the proposed model to equation 3.2, the current DP for this study. This provides a more "customizable" parameter depending on the type of specimens and multiaxial fatigue that is encountered.

With the proposed critical plane model in place, with an initial analysis showing great experimental results correlation from this study, this model should be examined further in more studies, with special emphasis in non-proportional loading, and the validity of the terms used as the addition to the current DP.

9. SUMMARY AND RECOMMEDATIONS

9.1. Summary

The purpose of this study was to examine the influence of the biaxiality ratio (BR) on multiaxial fatigue of DA 718. Two different fatigue models, the Pseudo Stress Parameter (PSP) and the Damage Parameter (DP), were evaluated against notch specimens which shared the same planar geometry, but differed in thickness, inducing different BRs. The PSP predicted a fatigue life benefit in the thick notch specimen with respect to the thin notch specimen, while the DP predicted a slight fatigue life reduction in the thick notch specimen with respect to the thin notch specimen.

The experimental results in this study indicated that a fatigue life benefit did exist for both forgings. However, the PSP overpredicted the fatigue life of the thick notch specimens for the V038 forging significantly, and uncertainty existed in the fatigue life of the thick notch specimens for the V036 forging. The DP for the study predicted a fatigue life reduction in the thick notch specimens for both forgings, which clearly did not follow the experimental results of the notch specimens. Therefore, the secondary stress needed to be accounted for, with a modification to the current DP.

A proposed critical plane model was presented, with an additional term that accounts for the secondary stress over the loading cycle, which is directionally normal to the plane created by the direction of the maximum shear strain range, and the direction of the stress normal to the critical plane. When compared against the experimental results of the notch specimens, the proposed critical plane model predicted promising results, with life predictions within one percent of the experimental average life values of both forgings for the thick notch specimens, using the thin notch specimens as the basis for the constant fit.

9.2. Recommendations

After completing this study, some recommendations have been made to further the study of this area of research.

The proposed model needs to be fit against other existing experimental data of different metallic materials to verify the validity of the model. This should include proportional and non-proportional loading, since non-proportional loading provides great challenges in correlating fatigue life with uniaxial and torsion data. It is possible that different terms and values could be used in the proposed model which shows better correlation of the data, and can be investigated further in new studies. Existing experimental data such as biaxial-tension data from Morrow [14] and Lefebvre [37] can and should be used to validate the proposed model.

Different materials can react differently to multiaxial fatigue loading, and should be investigated as well for correlation with the proposed critical plane model. This study used DA 718, but other materials such as steel, aluminum, and other superalloys such as Inconel 718 and Rene' 88 should be examined as they might react differently than the DA 718. If the model shows great promise with other existing experimental data, the constants for the proposed critical plane model can be fit for different materials.

The majority of this study was conducted in the LCF to transitional region of fatigue life, between 10,000 and 50,000 cycles. Equivalent stress parameters have shown great correlation in HCF experimental data, but different specimens at different fatigue life regimes should be used to generate constants and a curve fit for the proposed critical plane model that resembles the typical strain life equation, with a double power law to account for LCF and HCF effects.

Another factor to consider is the sign of the secondary stress component. In the proposed model, compressive secondary stresses would induce a higher first term, and therefore decrease

the fatigue life prediction, while tensile secondary stresses would produce a fatigue life benefit due to the reduction of the first term. Equivalent stress models, such as the PSP, produce a life benefit no matter what the sign of the secondary stress is, which is fundamentally different than the proposed model, and should be examined in further studies.

The crack propagation life of the notch specimens should be investigated, and considered in multiaxial fatigue analysis. Critical plane models are generally based upon crack nucleation and not crack propagation. Therefore, modeling, such as fracture mechanics, may be used to determine the crack propagation life once a critical crack has initiated in a component. Since the thickness was different between the two notch specimens, possible crack propagation life differences might exist. An initial analysis by GE was performed, and showed that the crack propagation life of the thick notch specimen was longer than the thin notch specimen, but the constants of the current DP were fit using failure lives.

REFERENCES

[1] B.-R. You and S.-B. Lee, "A critical review of multiaxial fatigue assessments of metals," *International Journal of Fatigue,* vol. 18, no. 4, pp. 235-244, May 1996.

[2] J. Goodman, Mechanics Applied to Engineering, London: Longman, Greens, and Co., 1899.

[3] Gerber, "Bestimmung der Zulosigne Spannugen in Eisen Constructionen," *Bayer. Arch. Ing. Ver.,* vol. 6, p. 101, 1874.

[4] L. F. Coffin Jr. and J. F. Tavemelli, "Experimental Support for Generalized Equation Predicting Low Cycle Fatigue," *Journal of Basic Engineering,* vol. 84, no. 4, pp. 533-537, 1962.

[5] S. S. Manson, "Discussion: L.F. Coffin Jr. and J.F. Tavelmelli, "Experimental Support for Generalized Equation Predicting Low Cycle Fatigue", Journal of Basic Engineering, Vol. 84, No.4, pg. 533-537, 1962," *Journal of Basic Engineering,* vol. 84, no. 4, pp. 537-541, 1962.

[6] D. F. Socie and G. B. Marquis, Multiaxial Fatigue, Warrendale, PA: Society of Automotive Engineers, 1999.

[7] D. F. Socie, "Critical Plane Approaches for Multiaxial Fatigue Damage Assessment," *Advances in Multiaxial Fatigue, ASTM STP 1191,* pp. 7-36, 1993.

[8] R. I. Stephens, A. Fatemi, R. R. Stephens and H. O. Fuchs, Metal Fatigue in Engineering, 2nd ed., John Wiley & Sons, Inc., 2001.

[9] A. Krgo, "Evaluation of Multiaxial Fatigue Life Predicition Methodologies for Ti-6Al-4V under High Cycle Fatigue Loading," M.S. Thesis, M.E. Dept., NDSU, Fargo, ND, 2000.

[10] A. R. Kallmeyer, A. Krgo and P. Kurath, "Evaluation of Multiaxial Fatigue Life Prediction Methodologies for Ti-6Al-4V," *Journal of Engineering Materials and Technology,* vol. 124, pp. 229-237, 2002.

[11] P. S. Maiya, "Effects of notches on crack initiation in low-cycle fatigue," *Materials Science and Engineering,* vol. 38, no. 3, p. 289–294, 1979.

[12] S. Bentachfine, G. Pluvinage, J. Gilgert, Z. Azari and D. Bouami, "Notch effect in low cycle fatigue," *International Journal of Fatigue,* vol. 21, no. 5, pp. 421-430, 1999.

[13] M. Sakane, S. Zhang and T. Kim, "Notch effect on multiaxial low cycle fatigue," *International Journal of Fatigue,* vol. 33, no. 8, pp. 959-968, 2011.

[14] D. L. Morrow, "Biaxial-Tension Fatigue of Inconel 718," Ph.D. Dissertation, M.E. Dept., Univ. Ill., Urbana, IL, 1988.

[15] G. Sines, "Behavior of Metals Under Complex Static and Alternating Stresses," in *Metal Fatigue*, G. Sines and J. L. Waisman, Eds., New York, McGraw-Hill Book Co., 1959, pp. 145-169.

[16] K. N. Smith, P. Watson and T. H. Topper, "A Stress-Strain Function for the Fatigue of Metals," *Journal of Materials,* vol. 5, no. 4, pp. 767-778, 1970.

[17] M. Erickson, A. Kallmeyer, E. Goodin, E. Torkelson and P. Kurath, "An Evaluation of Multiaxial Fatigue Data from Ti-6Al-4V using a Critical Plane Methodology," in *Proceedings of the 9th International Fatigue Congress*, Atlanta, 2006.

[18] Y. S. Garud, "A new approach to the evaluation of fatigue under multiaxial loadings," *Journal of Engineering Materials and Technology,* vol. 103, no. 2, pp. 118-125, 1981.

[19] Y. S. Garud, "Multiaxial Fatigue: A survey of the state-of-the-art," *Journal of Testing and Evaluation,* vol. 9, no. 3, pp. 165-178, 1981.

[20] F. Ellyin and D. Kujawski, "A Multiaxial Fatigue Criterion Including Mean-Stress Effect," in *Advances in Multiaxial Fatigue*, D. L. McDowell and R. Ellis, Eds., Philadelphia, ASTM, STP 1191, 1993, pp. 55-66.

[21] W. N. Findley, "A Theory for the Effect for Mean Stress on Fatigue of Metals Under Combined Torsion and Axial Load or Bending," *Journal of Engineering for Industry,* vol. 81, p. 301, 1959.

[22] M. W. Brown and K. J. Miller, "A Theory for Fatigue Under Multiaxial Stress-Strain Conditions," *Proceedings of the Institute of Mechanical Engineers,* vol. 187, p. 745, 1973.

[23] A. Fatemi and D. Socie, "A Critical Plane Approach to Multiaxial Fatigue Damage including Out-of-Phase Loading," *Fatigue & Fracture of Engineering Materials & Structures,* vol. 11, no. 3, pp. 146-165, 1988.

[24] D. F. Socie, "Multiaxial Fatigue Damage Models," *Journal of Engineering Materials and Technology,* vol. 109, pp. 293-298, 1987.

[25] H. Neuber, Kerbspannungstehre, Berlin: Springer, 1958.

[26] R. E. Peterson, Stress Concentration Factors, New York: John Wiley & Sons, Inc., 1974.

[27] H. Neuber, "Theory of Stress Concentration for Shear-Strained Prismatical Bodies with Arbitrary Nonlinear Stress Strain Laws," *Trans. ASME., Journal of Applied Mechanics,* vol. 28, p. 544, 1961.

[28] G. Glinka and K. Molski, "A Method of Elastic-Plastic Stress and Strain Calculation at a Notch Root," *Mat. Sci. Eng.,* vol. 50, p. 93, 1981.

[29] H. Murthy, P. T. Rajeev, T. N. Farris and D. C. Slavik, "Fretting Fatigue of Ti-6Al-4V Subjected to Blade/Disk Contact Loading," *Developments in Fracture Mechanics for the New Century, 50th Anniversary of Japan Society of Materials Science,* pp. 41-48, May 2011.

[30] A. R. Kallmeyer, "Estimation of HCF Threshold Stress Levels in Notched Components," in *High Cycle Fatigue*, New York, Elsevier, 2006, pp. 531-541.

[31] R. A. Naik, D. B. Lanning, T. Nicholas and A. R. Kallmeyer, "A critical plane gradient approach for the prediction of notch HCF life," *International Journal of Fatigue,* vol. 27, pp. 481-492, 2005.

[32] D. Leidermark, J. Moverare, K. Simonsson and S. Sjöström, "A combined critical plane and critical distance approach for predicting fatigue crack initiation in notched single-crystal superalloy components," *International Journal of Fatigue,* vol. 33, pp. 1351-1359, 2011.

[33] A. Carpinteri, A. Spagnoli, S. Vantadori and D. Viappiani, "A multiaxial criterion for notch high-cycle fatigue using a critical-point method," *Engineering Fracture Mechanics,* vol. 75, no. 7, p. 1864–1874, 2008.

[34] M. Hoffman and T. Seeger, "Estimating Multiaxial Elastic-Plastic Notch Stresses and Strains in Combined Loading," in *Biaxial and Multiaxial Fatigue, EGF3*, M. W. Brown and J. K. Miller, Eds., London, Mechanical Engineering Publications, 1989, pp. 3-24.

[35] D. Klann, S. Tipton and T. Cordes, "Notch Stress and Strain Estimation Considering Multiaxial Constrain," *SAE,* no. 930401, 1993.

[36] D. L. Morrow and P. Kurath, "Proportional Biaxial-Tension Low Cycle Fatigue of Inconel 718," in *Biaxial and Multiaxial Fatigue*, W. B. M. and J. M. K., Eds., London, Mechanical Engineering Publications, 1989, pp. 551-570.

[37] D. F. Lefebvre, "Hydrostatic Pressure Effect on Life Prediction in Biaxial Low-Cycle Fatigue," in *Biaxial and Multiaxial Fatigue*, M. W. Brown and K. J. Miller, Eds., London, Mechanical Engineering Publications, 1989, pp. 511-533.

[38] C. Zhang, "Low Cycle Fatigue Crack Initiation of Rotating Structures under Biaxial Stress States," in *Proceedings of ASME Turbo Expo 2009: Power for Land, Sea, and Air*, Orlando, 2009.

[39] M. N. Menton, P. T. Kantzos and D. J. Greving, "An innovative procedure for establishing lifing criteria for turbine disk bores under multiaxial states of stress," *International Journal of Fatigue,* no. 33, pp. 1111-1117, 2011.

[40] S. P. Feierabend, "A Critical-Plane Approach for Modeling Multi-Axial Fatigue Damage in High-Strength Alloys," M.S. thesis. Dept. ME, NDSU., Fargo, ND, 2007.

[41] D. D. Krueger, "The Development of Direct Age 718 for Gas Turbine Engine Disk Applications," in *Superalloy 718 - Metallurgy and Applications*, 1989, pp. 279-296.

APPENDIX

Listed below is a MATLAB script that calculates the critical plane and corresponding damage parameter based upon the XYZ stress and strain data.

```
%% Charles Adams
% Department of Mechanical Engineering
% North Dakota State University
% NDSU Damage Parameter Calculator - Shear strain range and largest DP
%% Begin Script
clc, clear;
%% Gather Stress and Strain Data
% Excel Data
SSData = xlsread('CriticalPlaneAnalysis.xlsx','Data','A2:L10000');
[TimeSteps c] = size(SSData);
clear c;
% Convert to tensoral strains
SSData(:,10:12) = SSData(:,10:12)./2;
%% Symbols
syms Nf;
%% Perform analysis
% Angles
Theta = 0:1:90;
ThetaRad = Theta.*pi./180;
Phi = 0:1:90;
PhiRad = Phi.*pi./180;
Angle = 0:1:90;
AngleRad = Angle.*pi./180;
Num = length(Angle);
% Parameters SS
SSRSS = 0;
SigmaTauMaxSS = 0;
TauMaxSS = 0;
TauRangeSS = 0;
DamageParameterSS = 0;
% Parameters GV
SSRGV = 0;
SigmaTauMaxGV = 0;
TauMaxGV = 0;
TauRangeGV = 0;
DamageParameterGV = 0;
% Constants
G = (1.15e7)/1000; %Shear Modulus - ksi
k = 0.574; %Constant DP
```

```
w = 0.433; %Constant DP
%Transformation Matrix
a = zeros(3);
% Begin critical plane analysis
for i = 1:Num
   for j = 1:Num
      % Transformation
      a(1,:) = [cos(ThetaRad(i))*sin(PhiRad(j)) sin(ThetaRad(i))*sin(PhiRad(j)) cos(PhiRad(j))];
      a(2,:) = [-sin(ThetaRad(i)) cos(ThetaRad(i)) 0];
      a(3,:) = [-cos(ThetaRad(i))*cos(PhiRad(j)) -sin(ThetaRad(i))*cos(PhiRad(j))
sin(PhiRad(j))];
      for l = 1:Num %Rotation of shear direction
         NormalStress = zeros(TimeSteps,1);
         ShearXY = zeros(TimeSteps,1);
         ShearXZ = zeros(TimeSteps,1);
         NormalStrain = zeros(TimeSteps,1);
         ShearStrainXY = zeros(TimeSteps,1);
         ShearStrainXZ = zeros(TimeSteps,1);
         for t = 1:TimeSteps
            % Stress
            NormalStress(t) = (SSData(t,1:3)*(a(1,1:3).^2)')+2*((SSData(t,4)*a(1,1)*a(1,2))...
                  +(SSData(t,5)*a(1,2)*a(1,3))+(SSData(t,6)*a(1,1)*a(1,3)));
            ShearXY(t) = SSData(t,1)*a(1,1)*a(2,1) + SSData(t,2)*a(1,2)*a(2,2) +
SSData(t,3)*a(1,3)*a(2,3)...
                  + SSData(t,4)*(a(1,1)*a(2,2)+a(1,2)*a(2,1)) +
SSData(t,5)*(a(1,2)*a(2,3)+a(1,3)*a(2,2))...
                  + SSData(t,6)*(a(1,3)*a(2,1)+a(1,1)*a(2,3));
            ShearXZ(t) = SSData(t,1)*a(1,1)*a(3,1) + SSData(t,2)*a(1,2)*a(3,2) +
SSData(t,3)*a(1,3)*a(3,3)...
                  + SSData(t,4)*(a(1,1)*a(3,2)+a(1,2)*a(3,1)) +
SSData(t,5)*(a(1,2)*a(3,3)+a(1,3)*a(3,2))...
                  + SSData(t,6)*(a(1,3)*a(3,1)+a(1,1)*a(3,3));
            % Strain
            NormalStrain(t) = (SSData(t,7:9)*(a(1,1:3).^2)')+2*((SSData(t,10)*a(1,1)*a(1,2))...
                  +(SSData(t,11)*a(1,2)*a(1,3))+(SSData(t,12)*a(1,1)*a(1,3)));
            ShearStrainXY(t) = 2*(SSData(t,7)*a(1,1)*a(2,1) + SSData(t,8)*a(1,2)*a(2,2) +
SSData(t,9)*a(1,3)*a(2,3)...
                  + SSData(t,10)*(a(1,1)*a(2,2)+a(1,2)*a(2,1)) +
SSData(t,11)*(a(1,2)*a(2,3)+a(1,3)*a(2,2))...
                  + SSData(t,12)*(a(1,3)*a(2,1)+a(1,1)*a(2,3)));
            ShearStrainXZ(t) = 2*(SSData(t,7)*a(1,1)*a(3,1) + SSData(t,8)*a(1,2)*a(3,2) +
SSData(t,9)*a(1,3)*a(3,3)...
                  + SSData(t,10)*(a(1,1)*a(3,2)+a(1,2)*a(3,1)) +
SSData(t,11)*(a(1,2)*a(3,3)+a(1,3)*a(3,2))...
                  + SSData(t,12)*(a(1,3)*a(3,1)+a(1,1)*a(3,3)));
         end
```

```
        q = [cos(AngleRad(l)) sin(AngleRad(l))];
        qb = [cos(AngleRad(l)-(pi/2)) sin(AngleRad(l)-(pi/2))];
        % Transform Shear Stresses on current plane
        DirShear = (q(1,1)^2).*ShearXY + (q(1,2)^2).*ShearXZ;
        DirShearStrain = (q(1,1)^2).*ShearStrainXY + (q(1,2)^2).*ShearStrainXZ;
        BShear = (qb(1,1)^2).*ShearXY + (qb(1,2)^2).*ShearXZ;
        % Analyze shear stress and strain
        TRange = max(DirShear)-min(DirShear);
        TMax = max(abs(DirShear));
%           BShearMax = max(abs(BShear));
        STMax = max(NormalStress.*abs(DirShear));
        SRange = max(DirShearStrain)-min(DirShearStrain);
        CalDP = ((TMax/1000)^(1-w)) * ((SRange*G)^w) * (1+k*(STMax/(TMax^2)));
        % Greatest shear strain range?
        if SRange > SSRSS
           TauRangeSS = TRange;
           TauMaxSS = TMax;
           SigmaTauMaxSS = STMax;
           SSRSS = SRange;
           DamageParameterSS = CalDP;
           CPAngleSS = [Theta(i); Phi(j); Angle(l)];
           BTauSS = BShear;
        end
        % Largest Damage Parameter
        if CalDP > DamageParameterGV
           TauRangeGV = TRange;
           TauMaxGV = TMax;
           SigmaTauMaxGV = STMax;
           SSRGV = SRange;
           DamageParameterGV = CalDP;
           CPAngleGV = [Theta(i); Phi(j); Angle(l)];
        end
      end
   end
end
%% Display Results
disp(DamageParameterSS);
```